

Comprehensive Comparison on Optical Properties of Samarium Oxide (Micro/nano) Particles Doped Tellurite Glass for Optoelectronics Applications

Azlan M.N (✉ azlanmn@fsmt.upsi.edu.my)

Universiti Pendidikan Sultan Idris <https://orcid.org/0000-0002-2792-4145>

Hajer S.S

University of Elmergib: Al Margeb University

Halimah Mohamed Kamari

Universiti Putra Malaysia

Umar S.A

Federal University Lafia

Zaid M.H.M

Universiti Putra Malaysia

Hisam R.

Universiti Teknologi MARA

Iskandar S.M

Universiti Sains Malaysia

Kenzhaliyev B.K

Satbayev University

Kassymova G.K

Satbayev University

Yusof N.N

Universiti Teknologi Malaysia

Original Research

Keywords: rare-earth oxide, nanoparticles, borotellurite glass, optical absorption

Posted Date: February 10th, 2021

DOI: <https://doi.org/10.21203/rs.3.rs-175843/v1>

License:   This work is licensed under a Creative Commons Attribution 4.0 International License.

[Read Full License](#)

Comprehensive comparison on optical properties of samarium oxide (micro/nano) particles doped tellurite glass for optoelectronics applications

^aAzlan M.N*, ^bHajer S.S, ^cHalimah M.K, ^dUmar S.A, ^eZaid, M.H.M., ^fHisam R., ^gIskandar S.M, ^hKenzhaliyev B. K., ⁱKassymova G.K., ^jYusof N.N.

^aPhysics Department, Faculty of Science and Mathematics, University Pendidikan Sultan Idris, 35900 Tanjong Malim, Perak, Malaysia;

^bPhysics department, Faculty of Science, Elmergib University, Port Street Al Khums 40414, Elmergib, Libya;

^cDepartment of Physics, Faculty of Science, Universiti Putra Malaysia, 43400, Serdang, Selangor, Malaysia;

^dDepartment of Physics, Faculty of Science, Federal University Lafia, Lafia, Nasarawa State, Nigeria;

^eFaculty of Applied Sciences, Universiti Teknologi MARA, 40450 Shah Alam, Selangor, Malaysia;

^fSchool of Physics, Universiti Sains Malaysia, 11800 USM, Penang, Malaysia;

^gInstitute of Metallurgy and Ore Beneficiation, Satbayev University, Almaty, Kazakhstan;

^hPhysics Department, AOMRG & Laser Centre, Faculty of Science, Universiti Teknologi Malaysia, 81310, Johor Bahru, Johor, Malaysia

Abstract. Rare-earth oxides microparticles doped tellurite-based glass have been studied extensively to improve the capability of optoelectronic devices. We report a detailed comparison between two sets of glass series containing samarium microparticles and nanoparticles denoted as ZBTSm-MPs and ZBTSm-NPs respectively. The two sets of glass have been successfully fabricated via melt-quenching technique with chemical formula $\{[(\text{TeO}_2)_{0.70} (\text{B}_2\text{O}_3)_{0.30}]_{0.7} (\text{ZnO})_{0.3}\}_{1-y} (\text{Sm}_2\text{O}_3 (\text{MPs/NPs}))_y$ with $y = 0.005, 0.01, 0.02, 0.03, 0.04$ and 0.05 mol fraction. The TEM analysis confirmed the existence and formation of nanoparticles in ZBTSm-NPs glasses. The density of ZBTSm-NPs glasses was found higher than ZBTSm-MPs glasses due to the distributions of nano-scale particles in tellurite glass network. There was a linear trend of increment in the refractive index in both sets of glass series along with the concentrations of dopants. The refractive index of ZBTSm-NPs glasses was found higher than ZBTSm-MPs glasses due to the shift in compactness of glass structure with nano-scale particles. In comparison, the absorption peaks of ZBTSm-MPs glasses were greater than ZBTSm-NPs glasses which were mainly due to the restriction of electrons mobility in glass network with nano-scale particles. The optical band gap energy in ZBTSm-NPs glasses was found greater than ZBTSm-MPs glasses which correspond to the widening of forbidden gap with nano-scale particles. The polarizability of ZBTSm-NPs and ZBTSm-MPs was found in non-linear trend along with dopant concentrations. Based on these findings, the improvement of optical properties have been made by introducing samarium oxide nanoparticles in tellurite glass which is beneficial for optoelectronic devices.

Keywords: rare-earth oxide; nanoparticles; borotellurite glass; optical absorption;

Introduction

Among chalcogenide oxide groups, tellurite oxide, TeO_2 is the most stable oxide. The effectiveness and usefulness of tellurite oxide for optoelectronics applications have motivated researchers around the world [1 – 4]. The recent study by **Peng et al.** proposed that tellurite oxide has been shown as a future material for a visible-band conversion laser fiber [5]. Furthermore, tellurite oxide is often transferred to many other glass oxides that support multiple compositions. **Fares et al.**, reported that tellurite oxide, TeO_2 consists of a lone pair electron at TeO_4 equatorial positions [6]. This occurrence will lead to the limitation of structural rearrangement and the formation of glass. As a result, pure tellurite oxide, TeO_2 glass is unstable and tend to crystallize [7]. However, in order to stabilize the formation of tellurite glass, it is necessary to incorporate modifiers such as alkali, alkali earth and metal oxides in tellurite glass network [8].

The best glass additive to be incorporated in tellurite glass network is borate oxide, B_2O_3 . The hygroscopic characteristic of a glass system may be reduced by combining the tellurite oxide and borate oxide [9]. Moreover, borotellurite glasses have broader infrared transmittance which is beneficial for optoelectronic devices. **Meera et al.**, observed that the borate glasses were made up of two tetrahedral (BO_4) and trigonal (BO_3) units [10]. The blending of these units would establish groupings of diborate, triborate, tetraborate and pentaborate [11]. In addition, **Manara et al.**, suggested that the inclusion of borate oxide in tellurite glass network may contribute to a stable structural unit as applied in the borosilicate glass system [12]. Tellurite glasses with small amount of borate oxide are composed of TeO_4 , BO_4 , and BO_3 groups. Such groups may result in a stable structure of tellurite glass and hence, improve its optical properties.

The improvement of mechanical strength, chemical resistance and the thermal expansion of the glass system can be made by introducing the Zinc oxide, ZnO in borotellurite glass network. **Khattak and Salim** stated that zinc oxide transforms TeO_4 (trigonal bipyramidal) to TeO_{3+1} polyhedra and TeO_3 (trigonal bipyramidal) coordination in tellurite glass network [13]. The lone pair in TeO_4 (trigonal bipyramidal) restricts the free movement of trigonal bipyramidal during cooling and melting processes. Zinc borotellurite glasses are stable in structure and contribute to the low crystal field of rare earth ions in the glass network [14].

Samarium oxide microparticles is frequently utilized in optical and photonic applications. A large number of studies were conducted to develop novel laser materials with the addition of samarium oxide. The establishment of zinc borotellurite glass doped with samarium oxide will therefore introduce alternative glass materials for possible uses in optoelectronic devices. As of now, several findings on samarium oxide microparticles doped tellurite glass are already researched [15, 16, 17]. Besides that, there are limited number of researches appears to be published on samarium oxide nanoparticles doped tellurite glass. Samarium oxide micro/nanoparticles vary in particle size. Samarium oxide nanoparticles comprises nano - size particles (< 100 nm), while samarium oxide forms micron-size particles. Samarium oxide nanoparticles have special features with respect to their composition, size and shape. These special features have an impact on the optical properties.

The contribution of this research is the development of novel glass materials for the improvement of optoelectronic devices. The aim of this study is to draw comparisons between the impact of samarium oxide microparticles (>100 nm) and samarium oxide nanoparticles (20 - 30 nm) inclusions in the tellurite glass system on their optical properties. Optical properties such as optical band gap, Urbach energy, refractive index, molar refraction, metallization criterion, electronic polarization and optical basicity of the glass system have been analyzed.

Methodology

The sets of glasses named as ZBTSm-MPs and ZBTSm-NPs were fabricated via melt-quenching technique. The compositions of the sets of glasses are as follows:

ZBTSm-MPs: $\{[(\text{TeO}_2)_{0.70}(\text{B}_2\text{O}_3)_{0.30}]_{0.70}(\text{ZnO})_{0.30}\}_{1-y}(\text{Sm}_2\text{O}_3)_y$;
 $y=0.005, 0.01, 0.02, 0.03, 0.04, 0.05$ mol%

ZBTSm-NPs: $\{[(\text{TeO}_2)_{0.70}(\text{B}_2\text{O}_3)_{0.30}]_{0.70}(\text{ZnO})_{0.30}\}_{1-y}(\text{Sm}_2\text{O}_3 \text{ nanoparticles})_y$;
 $y=0.005, 0.01, 0.02, 0.03, 0.04, 0.05$ mol%

The raw materials were obtained from manufactured company as follows:

The raw materials of tellurium (IV) oxide (TeO_2), (99.99%) - *Alfa Aesar*; Zinc oxide (ZnO), (99.99%) - *Alfa Aesar*; Boron oxide (B_2O_3), (98.5%) - *Alfa Aesar*; Samarium (III) oxide (>100 nm), (99.9%) - *Alfa Aesar*; Samarium nanoparticles (III) oxide (~15-30 nm), (99.9%) - *Alfa Aesar*

ZBTSm-MPs glasses consist of samarium oxide microparticles with particles size of > 100 nm. In the meantime, ZBTSm-NPs glasses comprise with samarium oxide nanoparticles with

particles size of ~30 nm. The mass of raw materials was weighed at 10 g and mixed thoroughly in platinum crucible. The platinum crucible containing the raw materials was heated in the electric furnace at 400 °C for 30 minutes. The raw materials were melted at 900 °C for 2 hours in the second furnace. The molten of raw materials was quenched into stainless-steel moulds which was pre-heated at 400 °C to prevent thermal stress. The obtained glass along with the stainless-steel moulds were annealed at 400 °C for 60 minutes to improve the mechanical strength. The glass sample was allowed to cool down at room temperature for 24 hours. The glass sample was polished with different kinds of sandpapers, 1500 grids, 1200 grids and 1000 grids to achieve the thickness of 2mm and smooth surfaces.

Some of the glass samples were crushed into a powder form to perform XRD analysis ($2\theta < 1.5^\circ$) and high-resolution transmission electron microscopy ((HRTEM) JEOL JSM-IT-100) with uncertainty of ± 0.02 nm. The glass samples with thickness of ~2mm were sent for optical absorption measurement by using UV-1650PC UV-Vis Spectrophotometer (Shimadzu). The range of wavelength for UV-Vis measurement is 200 nm – 900 nm with the uncertainty of ± 0.3 nm. Meanwhile, the density and molar volume of the glass samples were measured by utilizing Archimedes' principle with distilled water as immersion liquid with uncertainty of ± 0.001 g/cm³.

Results and Discussion

X-ray Diffraction and Transmission Electron Microscopy

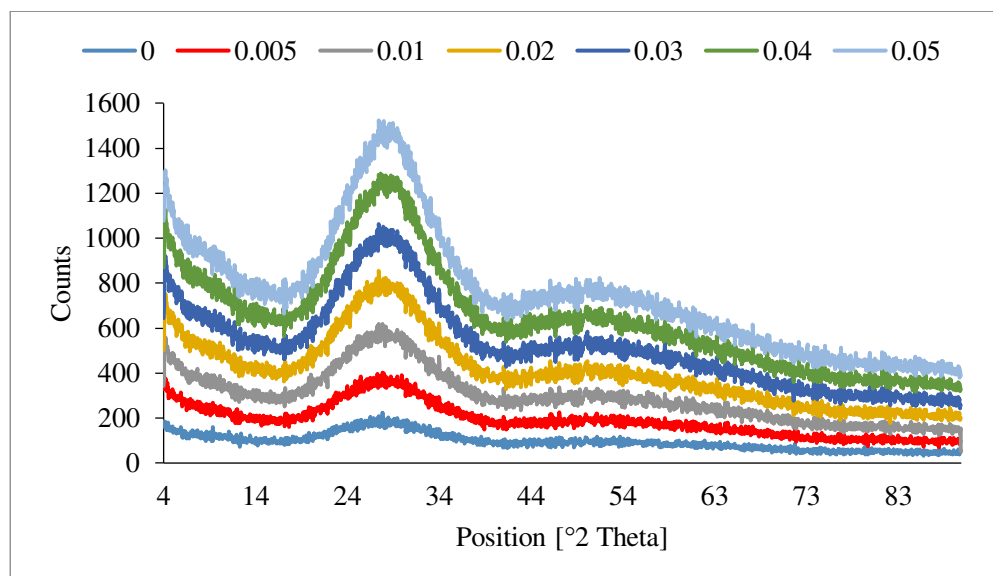


Fig.1a XRD spectra for ZBTsm-MPs glass series

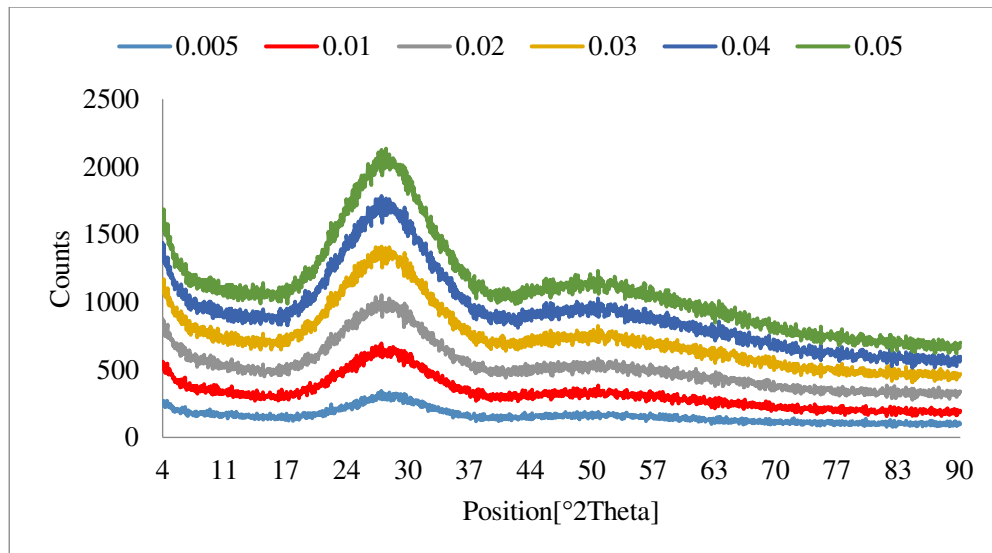


Fig.1b XRD spectra for ZBTSm-NPs glass series

The X-ray diffraction spectra for ZBTSm-MPs and ZBTSm-NPs glass series are plotted in the range of $10^{\circ} \leq \Theta \leq 80^{\circ}$ as shown in **Fig. 1a** and **Fig. 1b** respectively. The results indicate that the XRD pattern of ZBTSm-MPs and ZBTSm-NPs glass series reveals wide diffusion at lower scattering angles. This pattern proved the existence of long range structural disorder which correspond to the amorphous nature of the glass system. The absence of crystalline peaks show that the sets of glasses are completely in amorphous arrangement. The image in **Fig. 2** demonstrate the morphological structure of ZBTSm-NPs glass. The micrograph image of samarium oxide microparticles is not able to be displayed due to restriction in the TEM instrument that disallows the analysis of micro-size particles.

The shape of samarium oxide nanoparticles in raw materials is in three-dimensional shape. Meanwhile, the shape of samarium oxide nanoparticles is unchanged after the glass formation as shown in **Fig. 2**. The average particle size of raw materials for samarium oxide nanoparticles is 12.54 nm. After the glass formation, the size of samarium oxide nanoparticles is slightly enhanced with a diameter of approximately 23.53 nm. The growing size of nanoparticles in the glass structure is due to the Ostwald ripening effect via the dissolution of particles with small radius and re-precipitation with a large radius [18]. In addition, the size of the particles in the glass network may be increased due to the following factors:

1. Coagulation process: small particles may disappear by collisions as the nanoparticles migrate within the glass system, resulting in larger particles [19].

2. Particle coalescence: larger particle formation owing to strong chemical or physical bonding [19].

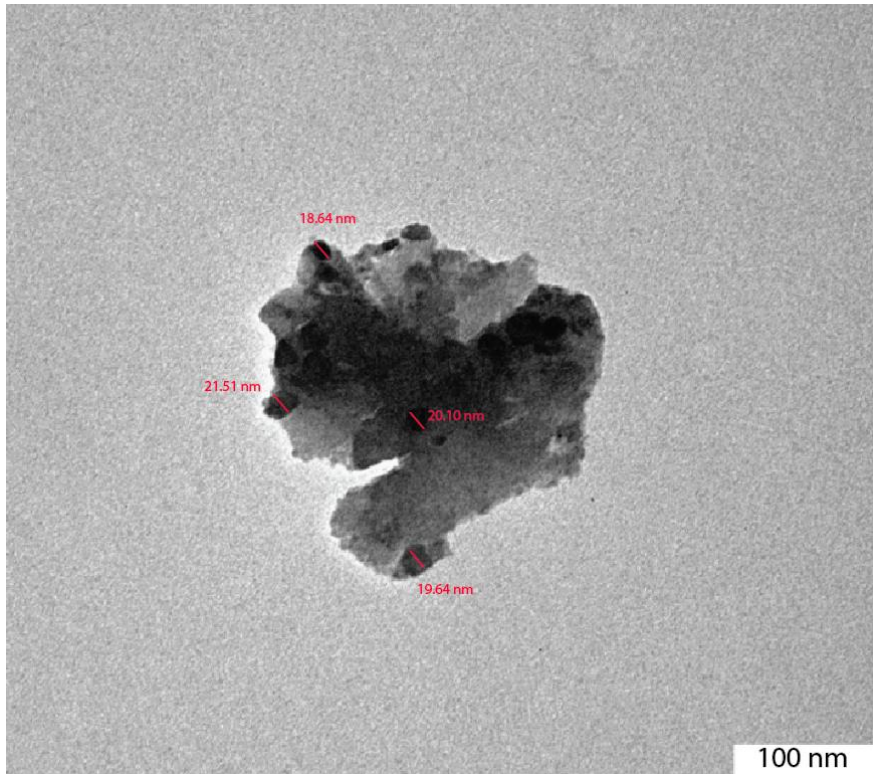


Fig. 2 TEM micrograph image for ZBTSm-NPs glass series

Density and molar volume

The density of ZBTSm-MPs and ZBTSm-NPs glasses are listed in **Table 1** and **Table 2** and shown in **Fig. 3**. The major difference between the two sets of glass series is that the ZBTSm-MPs glasses are less dense than the ZBTSm-NPs glasses. **Greenwood** stated that the small size of particles have high tendency to disperse throughout the materials with high degree of homogeneity and solubility [20]. Moreover, **Toy et al.**, confirmed that the small size of particles affects the distribution of the particles by reducing the density of materials [21]. **Nanda et al.**, proposed that the size of particles affect the cohesive energy by lowering its number if the particles is in small size [22]. Hence, the reduction of cohesive energy may increase the number of density of the glass system. Moreover, the small size particles has low number of volume in unit cells which contributes to the rise of density.

The similarity between the sets of glasses can be found in the average trend of density along with the dopant concentration. It is clearly seen that the density increases with the increasing number of dopant concentration. The formation of non-bridging oxygen in tellurite glass network is the main reason of such trend. Samarium consist of trivalent ions which produce three non-bridging oxygen by breaking the chain of bridging oxygen. The crosslinking of tellurite glass network will be degraded by the formation of non-bridging oxygen which leads to the increment of the density. Hence, the concentrations of samarium ions have major roles in determining the density of the glass system.

The comparison in molar volume between the sets of glasses can be seen in **Fig. 4** and tabulated in **Table 1 and Table 2**. **Fig. 4** shows that the molar volume of ZBTSm-MPs glasses is higher than ZBTSm-NPs. The nanoparticles distribution in tellurite glass network leads to the decrease of molar volume as the glass network become more compact [23]. Moreover, the molar volume is the reciprocal of the density which contributes to the shift of molar volume in both set of glasses. The two sets of glass series show similarity in the trend of molar volume along with the dopant concentrations. The increasing values of molar volume for both ZBTSm-MPs and ZBTSm-NPs glasses are mainly due to the difference in atomic radius of samarium ($r = 175$ pm) which is much higher than tellurium ($r = 140$ pm). Hence, the molar volume of tellurite glass will be expanded along with dopant concentrations. The decrease in molar volume at 0.05 mole fraction of both sets of glasses may be due to the structural rearrangement during the glass formation.

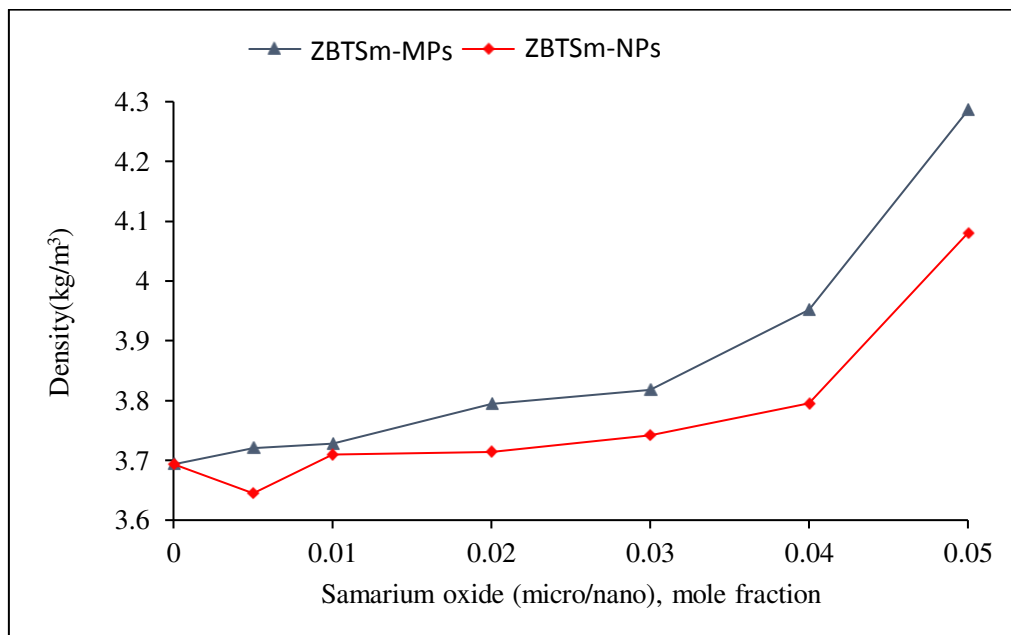


Fig. 3 Density for ZBTSm-MPs and ZBTSm-NPs glass series

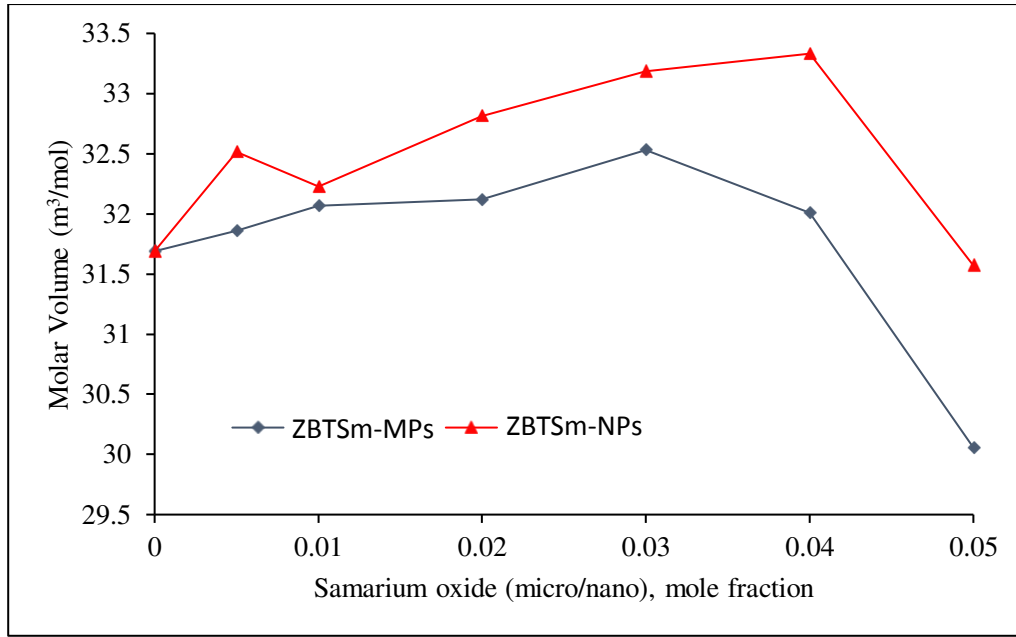


Fig. 4 Molar volume for ZBTsm-MPs and ZBTsm-NPs glass series

Table 1: Density and molar volume of samarium doped zinc borotellurite glass system

Mol fraction	Density (kg/m ³)	Molar Volume (m ³ /mol)
0.000	3.693	31.689
0.005	3.720	31.857
0.010	3.728	32.067
0.020	3.794	32.118
0.030	3.817	32.530
0.040	3.951	32.010
0.050	4.285	30.057

Table 2: Density and molar volume of samarium nanoparticles doped zinc borotellurite glass system

Mol fraction	Density (kg/m ³)	Molar Volume (m ³ /mol)
0.005	3.644	32.515
0.010	3.709	32.227
0.020	3.714	32.810
0.030	3.741	33.187
0.040	3.795	33.331
0.050	4.080	31.570

Refractive index

Refractive index is extremely important parameter to develop the optoelectronics applications such as optical waveguides, optical filters, optical adhesives and optical fiber. **Fig. 5** revealed the pattern of refractive index along with dopant concentrations for ZBTSm-MPs and ZBTSm-NPs glass series. Meanwhile, **Table 3 and Table 4** listed the specific values of refractive index for both sets of glasses. The range of refractive index for ZBTSm-MPs glass series is found in between 1.774 – 1.924, meanwhile ZBTSm-NPs glass series is located in between 1.716 – 1.740. **Fig. 5** revealed that the refractive index of ZBTSm-NPs is higher than ZBTSm-MPs.

The shift in refractive index can be explained by the following factors; a. density, b. non-bridging oxygen, c. polarizability, d. coordinate number [24]. The high value of refractive index is due to the high compactness in ZBTSm-NPs glasses structure than ZBTSm-MPs glasses. The small particles reduce the interstitial spaces between the atoms and limit the propagation of photon energy in the glass network [25]. Meanwhile, both ZBTSm-MPs and ZBTSm-NPs glass series are found similar in the trend of refractive index along with dopant concentrations. The rare-earth ions increase the number of non-bridging oxygen in the glass structure that affect the change in refractive index [26]. It is known that the non-bridging oxygen consists of lone pair electrons which are less tightly bound to the nuclear charge. Hence, the high polarizability of lone pair electrons enhances the number of refractive index.

Moreover, the presence of rare-earth ions may reduce the average cross-linking density which enhance the value of refractive index [27]. Large polarizability of the glass system minimizes the velocity of light propagation in a medium which, in turn, generates a high refractive index [28]. Hence, the increase in refractive index is also corresponded to the high value of polarizability in tellurite glass.

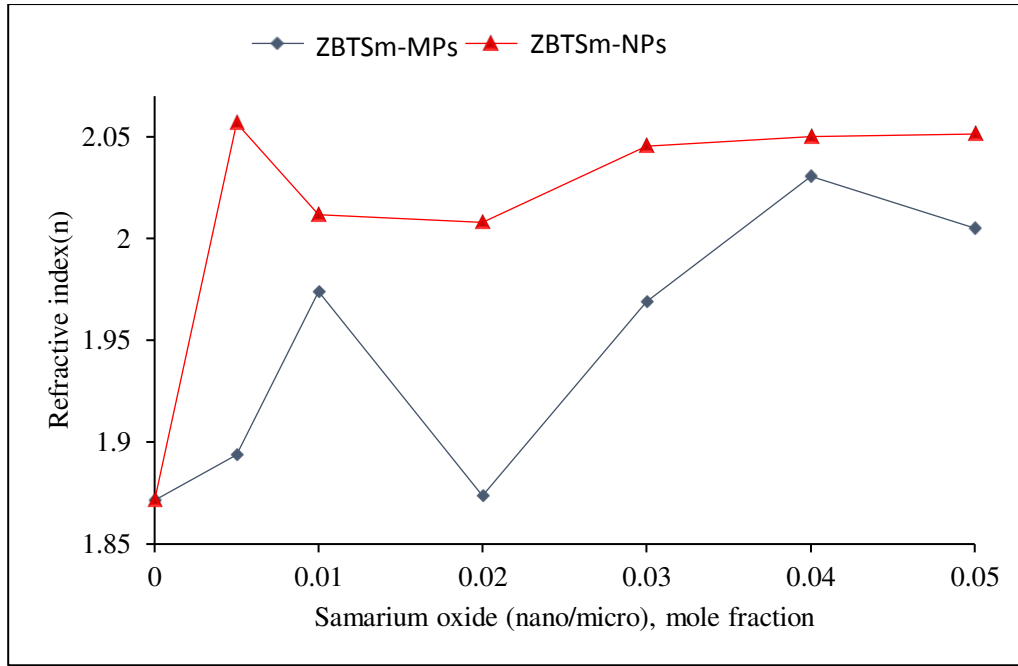


Fig. 5 Refractive index for ZBTsm-MPs and ZBTsm-NPs glass series

Table 3. Refractive index, molar refraction and polarizability for ZBTsm-MPs glass series

Mol fraction	Refractive index(n)	Molar refraction (R_M) (cm^3)	Polarizability(α_e) ($\times 10^{-24}$) (cm^3)
0.000	1.871	14.412	5.716
0.005	1.893	14.749	5.849
0.010	1.974	15.752	6.248
0.020	1.873	14.633	5.804
0.030	1.968	15.923	6.315
0.040	2.030	16.327	6.487
0.050	2.005	15.080	5.981

Table 4. Refractive index, molar refraction and polarizability for ZBTSm-NPs glass series

Mol fraction	Refractive index(n)	Molar refraction (R_M) (cm^3)	Polarizability(α_e) ($\times 10^{-24}$) (cm^3)
0.005	2.056	16.858	6.686
0.010	2.011	16.239	6.018
0.020	2.007	16.492	6.541
0.030	2.045	17.087	6.779
0.040	2.050	17.211	6.828
0.050	2.051	16.313	6.472

Optical absorption and band gap energy

The optical absorption versus wavelength spectra for ZBTSm-MPs and ZBTSm-NPs glasses are shown in **Fig. 6** and **Fig. 7** respectively. The non-existence of sharp absorption edge reveals the glassy state of the glass system. There are several sharp peaks revealed in the absorption spectra indicating the excitation of electrons from the ground state to several energy levels. The sharp peaks are located at 357, 405, 473, 955, 1084, 1229, 1381, 1480, 1533, 1590 and 1645 nm which correspond to the absorption of photon energy from the ground state $^6H_{5/2}$ to excited state; $^4D_{3/2}$, $^4M_{19/2}$, $^4I_{11/2}$, $^6F_{11/2}$, $^6F_{9/2}$, $^6F_{7/2}$, $^6F_{5/2}$, $^6F_{3/2}$, $^6H_{15/2}$, $^6F_{1/2}$ and $^6H_{13/2}$

The sharp peaks of ZBTSm-MPs glasses are found more intense than ZBTSm-NPs glasses. The reduction of absorption intensity in ZBTSm-NPs glasses may be due to the restriction of valence electrons which is closer to the nuclear charge [29]. The small particles may have smaller distance of valence electrons to the nuclear charge which reduce the mobility of electrons. The absorption coefficient values can be calculated based on the absorption edge by the following formula:

$$\alpha(\lambda) = 2.303 \frac{A}{d} \quad (1)$$

Where A corresponds the absorbance and d is the thickness of the glass samples. From the above formula, it is clear that the thickness of the glass sample affects the absorption coefficient value. Hence, the thickness of the glass samples is set to 2mm for all glass samples to prevent the errors from the data. The absorbance of the glass sample influences the absorption coefficient with direct proportional behavior to the value of absorption coefficient. It can be

seen from the figure that the absorption edge shifts to the longer wavelength along with dopant concentrations. This trend may be due to the less rigidity in the glass system [30].

The optical band gap energy is determined by applying Mott-Davis equation as follows [31]:

$$\alpha(\omega) = \frac{B(\hbar\omega - E_{opt})^n}{\hbar\omega} \quad (2)$$

B is the constant, $\hbar\omega$ defined the photon energy, E_{opt} correspond to the energy band gap, and n determines the type of transitions.

The indirect band gap is determined by applying $n = 2$ while the direct band gap is when $n = \frac{1}{2}$. Direct transition is a process where the electrons are transmitted to conduction band directly from the valance band. This transition is done by transition-dipole moments and surface electric fields [32]. On the other hand, the indirect transition is a process where the photo-excited electrons are excited into intermediate state and transferred to conduction band. The extrapolation of the direct and indirect graph for ZBTSM-MPs and ZBTSM-NPs are shown in **Fig. 8**, **Fig. 9**, **Fig. 10** and **Fig. 11** respectively. The optical band gap values depend on the structural variations in the glass matrix and the type of dopants.

Fig. 12 and **Fig. 13** illustrates the direct and indirect optical band gap for ZBTSM-MPs and ZBTSM-NPs glasses respectively, meanwhile, **Table 5** listed the specific values of direct and indirect optical band gap. It is clearly seen from **Fig. 10** that the optical band gap of ZBTSM-NPs is higher than ZBTSM-MPs. The small particles restrict the mobility of valence electrons and hence, widen the optical band gap. **Gupta et al.**, proposed that the optical properties of materials are highly dependent on the particle size [33]. The previous reports proved that the optical band gap is size dependent and there is an increase in the band gap of the semiconductor with a reduction in the particle size [34, 35]. The small particles of samarium oxide reduce the number of overlapping orbitals and hence, widen the gap between valence and conduction bands.

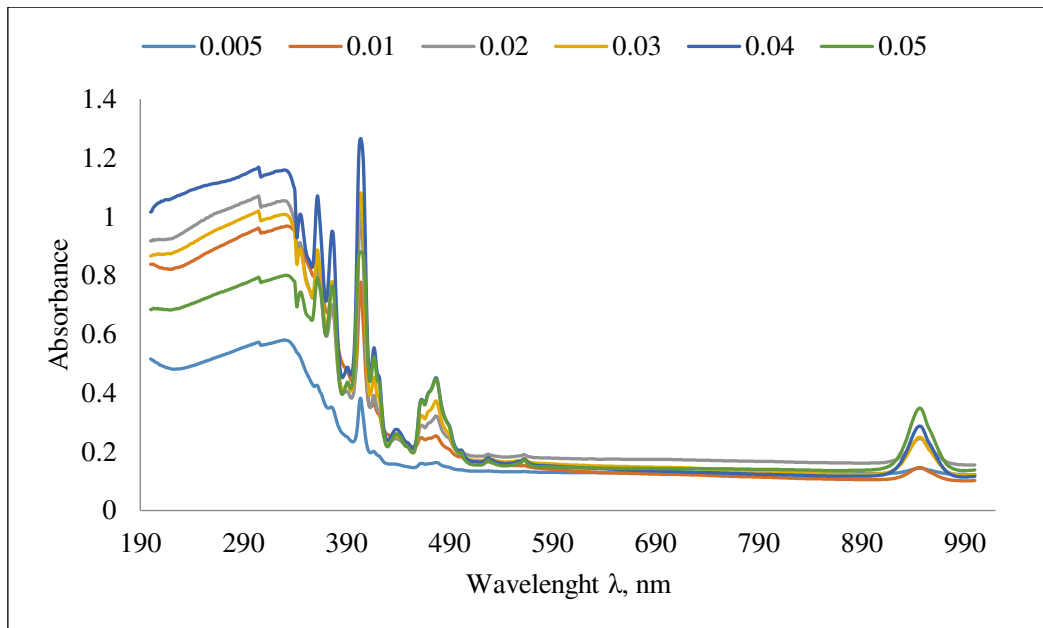


Fig. 6 Optical absorption for ZBTSm-MPs glass series

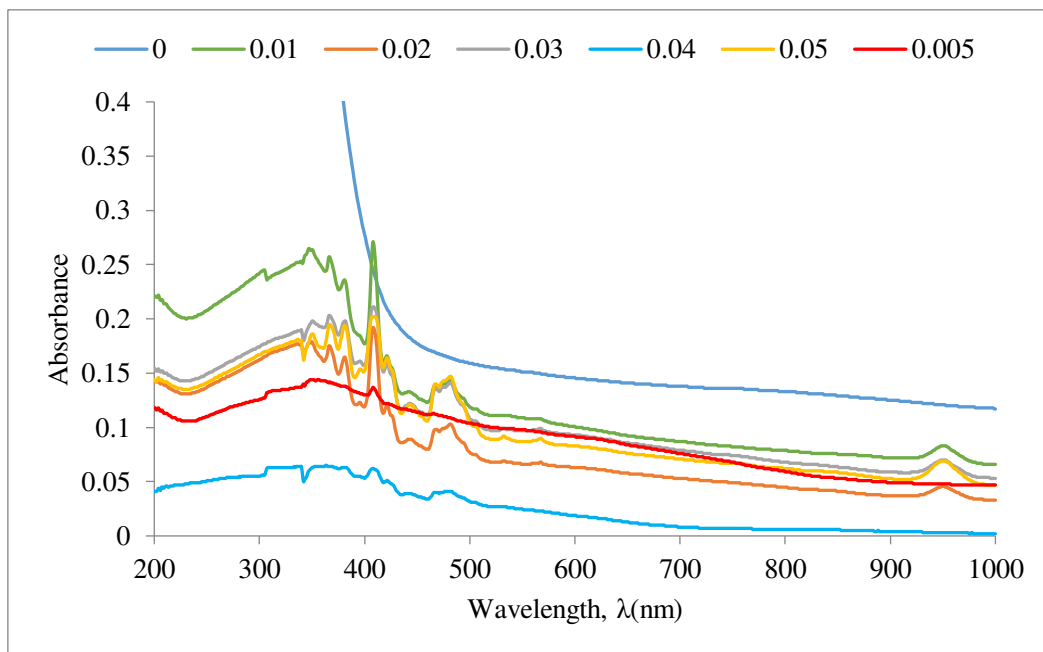


Fig. 7 Optical absorption for ZBTSm-NPs glass series

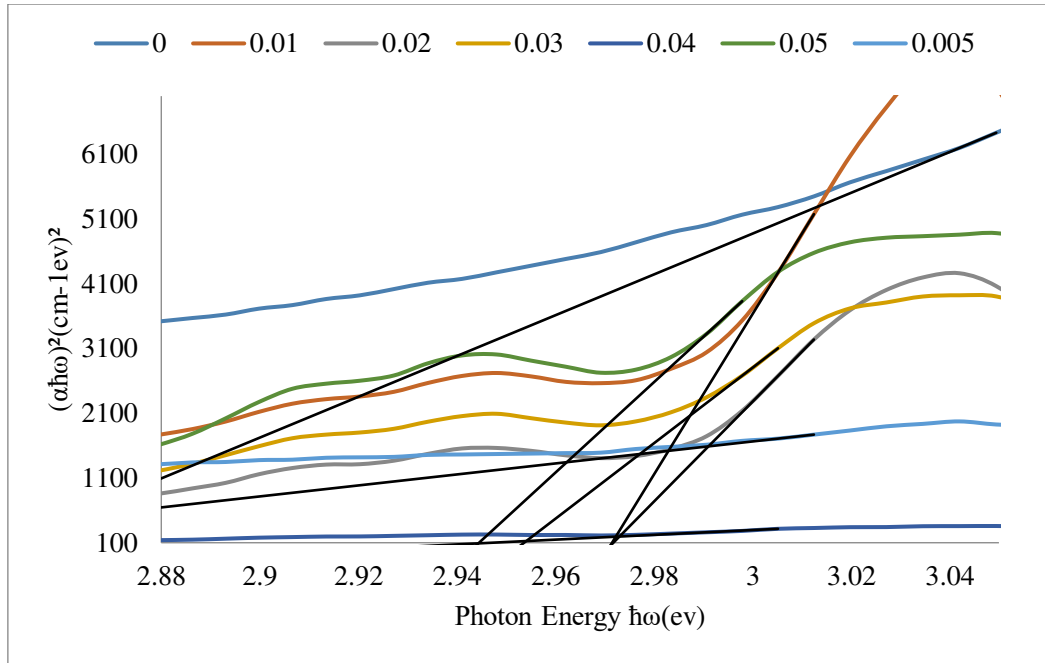


Fig.8: Plot of $(\alpha\hbar\omega)^2$ against photon energy $\hbar\omega$ of ZBTSm-MPs for direct band gap measurement

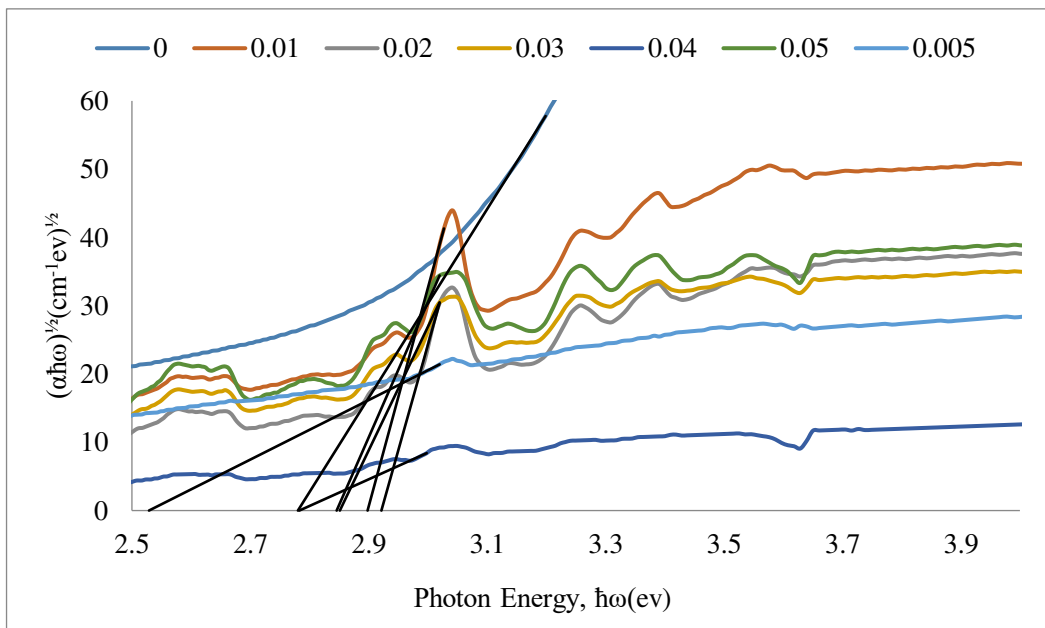


Fig. 9 Plot of $(\alpha\hbar\omega)^{1/2}$ against photon energy $\hbar\omega$ of ZBTSm-MPs for indirect band gap measurement

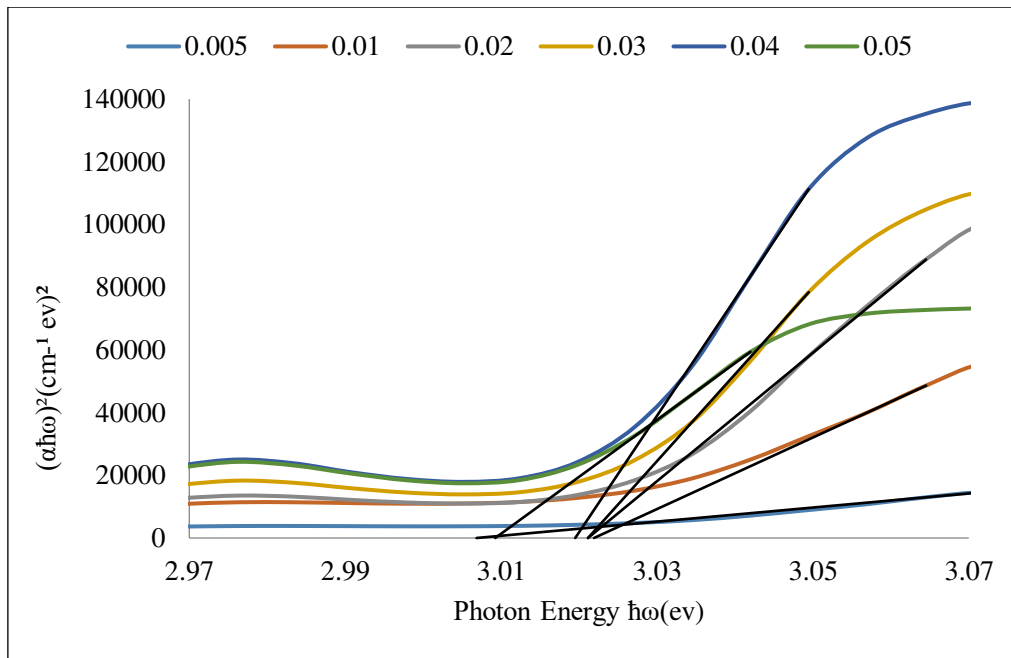


Fig. 10 Plot of $(\alpha\hbar\omega)^2$ against photon energy $\hbar\omega$ of ZBTSm-NPs for direct band gap measurement

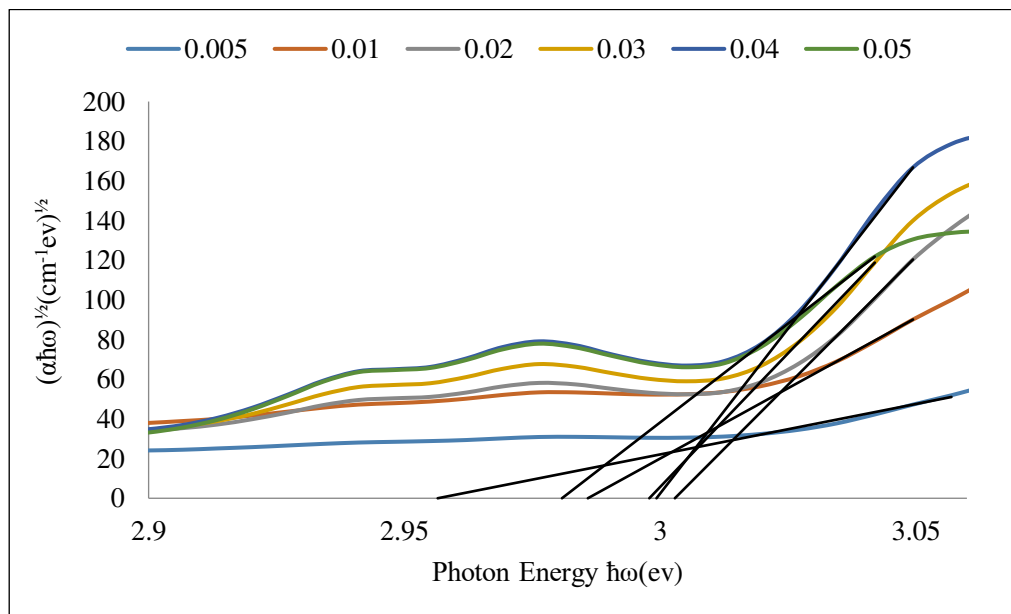


Fig. 11 Plot of $(\alpha\hbar\omega)^{1/2}$ against photon energy $\hbar\omega$ of ZBTSm-NPs for indirect band gap measurement

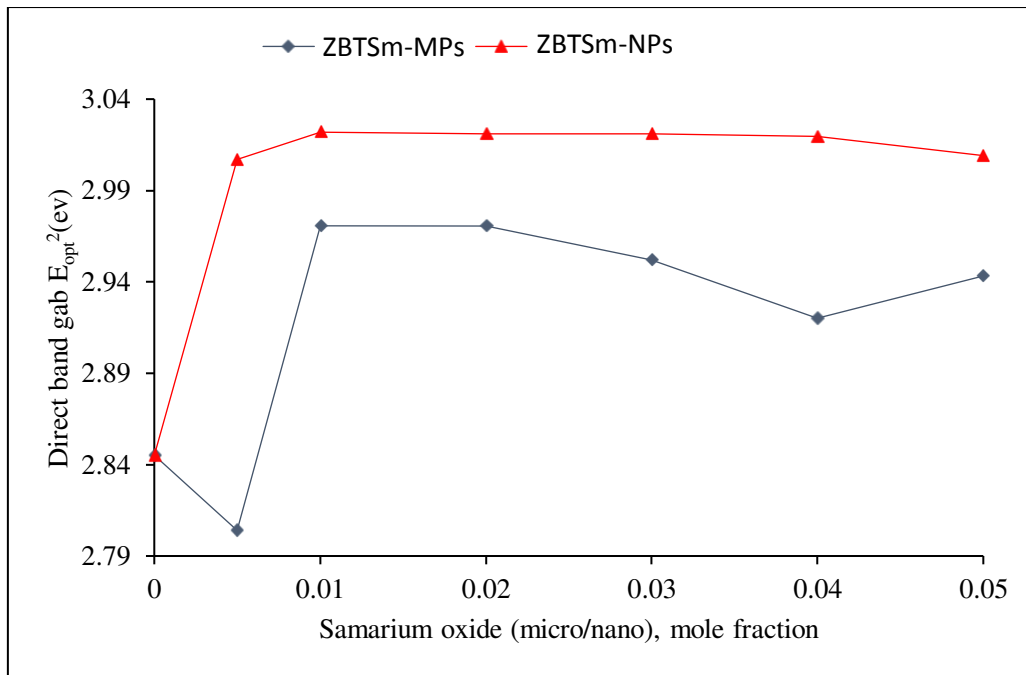


Fig. 12 Direct optical band gap for ZBTSm-MPs and ZBTSm-NPs glass series

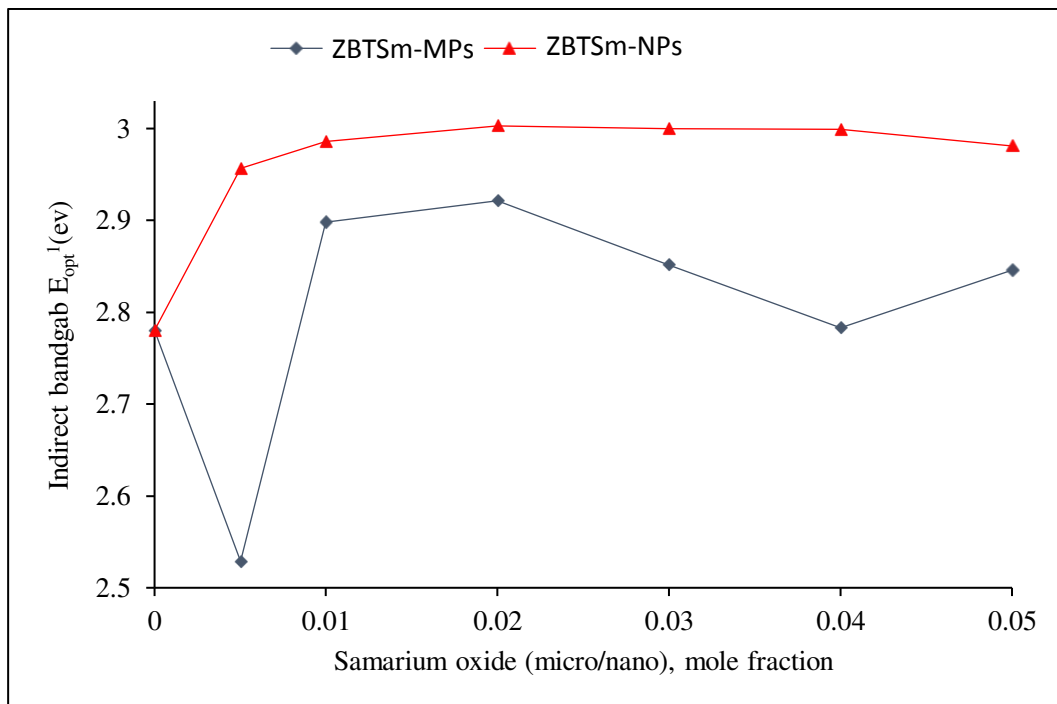


Fig. 13 Indirect optical band gap for ZBTSm-MPs and ZBTSm-NPs glass series

Table. 5 Direct and indirect optical band gap for ZBTSm-MPs and ZBTSm-NPs glass series

Mol fraction	Indirect band gap, E_{opt}^1 (eV)	Direct band gap, E_{opt}^2 (eV)
<i>ZBTSm-MPs</i>		
0.000	2.780	2.845
0.005	2.528	2.804
0.010	2.898	2.970
0.020	2.921	2.970
0.030	2.851	2.951
0.040	2.782	2.920
0.050	2.845	2.943
<i>ZBTSm-NPs</i>		
0.005	2.956	3.006
0.010	2.985	3.021
0.020	3.002	3.021
0.030	2.991	3.021
0.040	2.999	3.019
0.050	2.980	3.009

3.5 Molar refraction and polarizability

The estimation of the non-linear optical response for glass materials can be made by computing the value of polarizability. The exposure of an intense light beam in glass materials leads to polarization of ions and optical non-linearity. Polarization of rare-earth ions in glass materials affect greatly on optical properties such as absorption, refractive index and electro-optical effect. The computation of polarizability, α_e can be made by considering the refractive index values as follows [36]:

$$\frac{n^2-1}{n^2+2}(V_m) = \frac{4}{3}\pi N\alpha_e \dots \dots \dots (3)$$

Here V_m is the molar volume, N correspond to the Avogadro number and α_e denotes the polarizability. The equation (3) can be altered by introducing the density of the glass system as follows [36]:

$$\frac{n^2-1}{n^2+2}\left(\frac{M}{\rho}\right) R \dots \dots \dots (4)$$

Here, R is the refractivity of glass materials. The molar refraction, R_M , can be calculated by the following formula [36]:

$$\frac{n^2-1}{n^2+2} \left(\frac{M}{\rho} \right) = R_M \dots \dots \dots (5)$$

Here M is the molecular weight and $\frac{M}{\rho}$ is the molar volume of glass materials. Based from equation 4 and 5, the value of refractivity, R_M and refractive index, n depends on the polarizability of glass materials. Molar refractivity is proportional to the polarizability of the samarium ions. Molar refractivity, R_M can be obtained by the following expression:

$$R_M = (V_m) \frac{n^2-1}{n^2+2} \dots \dots \dots (6)$$

Where V_m is the molar volume and n is the refractive index.

Polarizability and molar refraction values for ZBTSM-MPs and ZBTSM-NPs glass series are illustrated in and **Fig. 14** and **Fig. 15** and tabulated in **Table 4** and **Table 5** respectively. It can be seen from the **Fig. 14** and **Fig. 15** that there are sudden decrease in molar refractivity and polarizability at 0.02 mol% and 0.05 mol% for ZBTSM-MPs glass series. Meanwhile, it is found that the molar refractivity and polarizability for ZBTSM-MPs glass series decrease at 0.01 mol%. Based on these variations, it can be justified that the data is in non-linear trend but slightly increases. The variations of molar refractivity and polarizability are related to the role of zinc oxide which breaks the Te–O–Te bridging oxygen and thus, form the Te–O–Zn²⁺ non-bridging oxygen [37].

Furthermore, certain amount of samarium oxide might affect the formation of Te–O–Zn²⁺ non-bridging oxygen. The high number of non-bridging oxygen increases the ionicity of glass materials and reduce the bond energy. The non-bridging oxygen is more likely to polarize compare to bridging oxygen. Besides that, the dual nature of zinc oxide may lead to the shifts of molar refraction and polarizability at 0.02 mol% and 0.05 mol% of samarium oxide. The high number of coordination number in samarium ions may result to the structural shifts from symmetric (TeO₄)⁴⁻ to asymmetric (TeO₃)²⁻ structure which gives significant effect on the optical properties [38]. Furthermore, the Sm²⁺ ions are changed to Sm³⁺ ions after the glass formation by getting one electron from the oxygen via redox reaction [39]. This trend will subsequently increase the number of outer electrons and creation of new bonds with oxygen atoms.

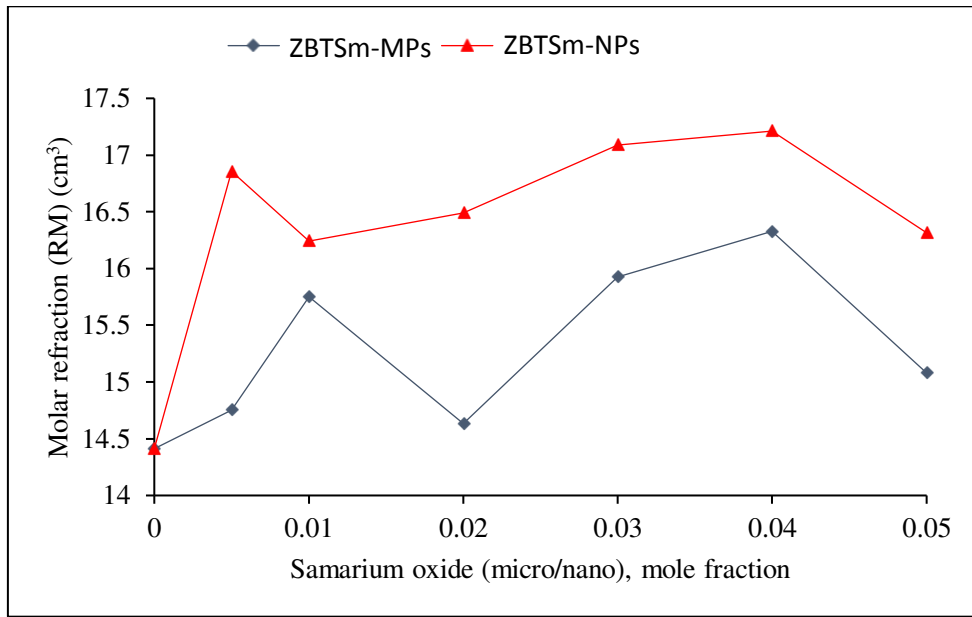


Fig. 15 Molar refraction for ZBTSm-MPs and ZBTSm-NPs glass series

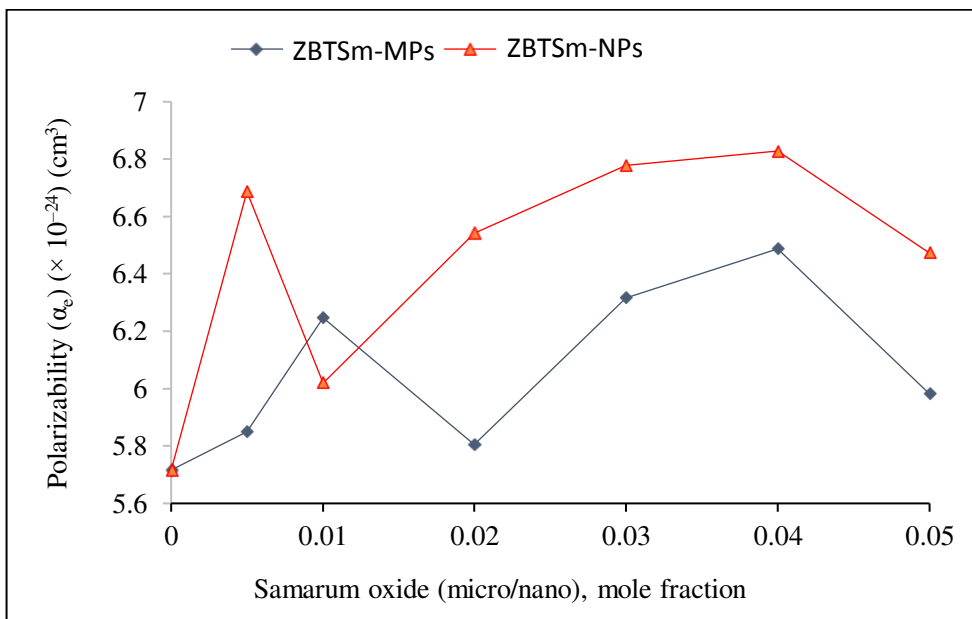


Fig. 16 Polarizability for ZBTSm-MPs and ZBTSm-NPs glass series

Conclusions

The two sets of glass series denoted as ZBTSm-MPs and ZBTSm-NPs were fabricated by using conventional melt-quenching method. The significant outcomes on structural, physical and optical properties between ZBTSm-MPs and ZBTSm-NPs glasses are as follows:

- The average size of nanoparticles in ZBTSm-NPs was found in the range ~23.53 nm.

- The density of ZBTSM-NPs glasses is found less than ZBTSM-MPs glasses due to the increasing compactness in glass structure with the existence of nano-scale particles
- The refractive index of ZBTSM-NPs glasses is found higher than ZBTSM-MPs glasses which is caused by the shift in density.
- The absorption peaks of a ZBTSM-MPs glasses are two times intense than ZBTSM-NPs glasses which correspond to the restriction of electrons in nano-scale particles.
- The optical band gap of ZBTSM-NPs glasses is found greater than ZBTSM-MPs glasses which is mainly due to widening of forbidden gap with nano-scale particles
- The non-linear trend of polarizability is found in both set of glasses due to the role of zinc oxide in tellurite glass system

Hence, based from these results the proposed glasses might be useful to develop the optoelectronic devices.

Acknowledgements

This research was financially supported by Skim Geran Penyelidikan Fundamental (FRGS) Fasa 1/2018 (**Grant code: 2019-0006-102-02**). The authors would like to thank the following institutions for equipment support: Faculty of Science and Mathematics, Universiti Pendidikan Sultan Idris and Faculty of Science and Universiti Putra Malaysia.

References:

1. R. Hisam, A.K. Yahya, Elastic moduli, optical and electrical properties of mixed electronic-ionic $30\text{Li}_2\text{O}-4\text{MoO}_3-(66-x)\text{TeO}_2-x\text{V}_2\text{O}_5$ tellurite glass system, Results in Physics, Volume 13, 2019, 102219
2. Mostafa, A.M.A., Issa, S.A., Zakaly, H.M., Zaid, M.H.M., Tekin, H.O., Matori, K.A., Sidek, H.A.A. and Elsaman, R., 2020. The influence of heavy elements on the ionizing radiation shielding efficiency and elastic properties of some tellurite glasses: Theoretical investigation. Results in Physics, 19, p.103496.
3. S.N. Nazrin, M.K. Halimah, F.D. Muhammad, A.A. Latif, S.M. Iskandar, A.S. Asyikin, Experimental and Theoretical Models of Elastic Properties of Erbium-doped Zinc Tellurite Glass System for Potential Fiber Optic Application, Materials Chemistry and Physics, 2020, 123992

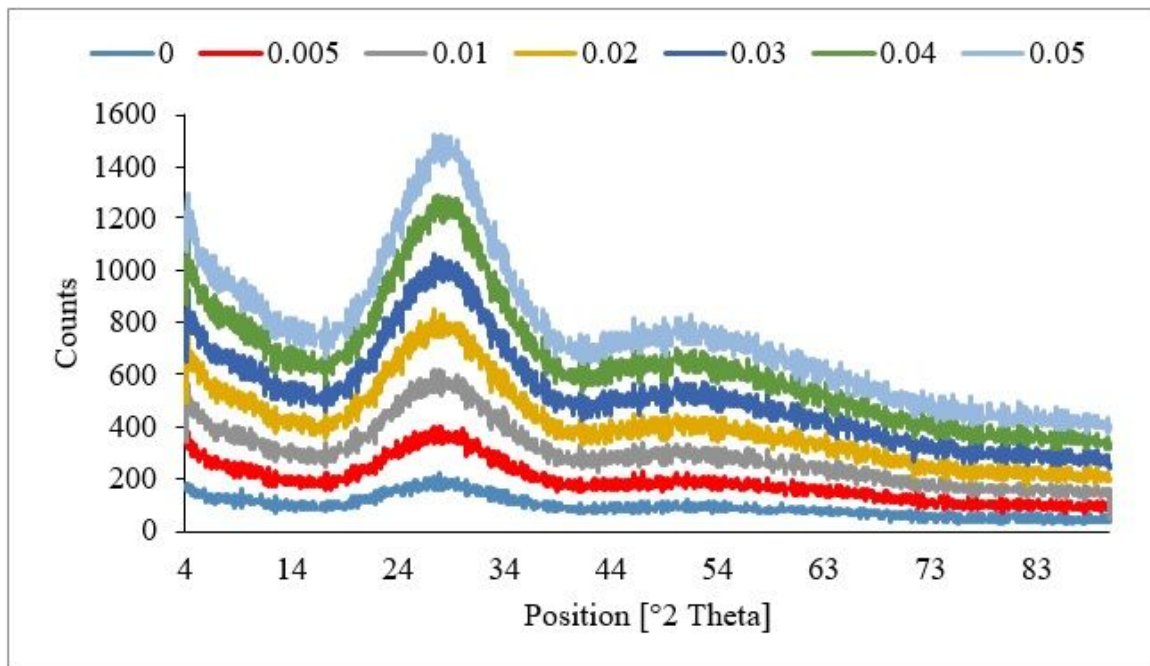
4. R.A. Tafida, M.K. Halimah, F.D. Muhammad, K.T. Chan, M.Y. Onimisi, A. Usman, A.M. Hamza, S.A. Umar, Structural, optical and elastic properties of silver oxide incorporated zinc tellurite glass system doped with Sm³⁺ ions, *Materials Chemistry and Physics*, Volume 246, 2020, 122801
5. Peng S., Wu L., Wang B., Yang F., Qi Y., and Zhou Y., “Intense visible upconversion and energy transfer in Ho³⁺/Yb³⁺ codoped tellurite glasses for potential fiber laser,” *Opt. Fiber Technol.*, (2015). Vol. 22, pp. 95–101
6. Fares H., Jlassi I., Elhouichet H., and Férid M., “Investigations of thermal, structural and optical properties of tellurite glass with WO₃ adding,” *J. Non. Cryst. Solids*, (2014). Vol. 396–397, pp. 1–7
7. Ning Ding, Jinlong Diao, Dongwei Zhang, Tao Zheng, Jingwen Lv, Spectroscopic properties of Yb³⁺ and Nd³⁺ co-doped tellurite glass for 1.0 μm laser application, *Ceramics International*, Volume 46, Issue 16, Part A, 2020, Pages 25633-25637
8. Mohammed Aliyu, A., & Ahmed, N. E. (2019). Structure and Physical Properties of 30MgSO₄-(70-x) P₂O₅-xSm₂O₃ glasses. *EDUCATUM Journal of Science, Mathematics and Technology*, 6(2), 22-34
9. Umar, S. A., & Ibrahim, G. G. (2020). Theoretical Elastic Moduli of TeO₂ – B₂O₃ – SiO₂ Glasses. *EDUCATUM Journal of Science, Mathematics and Technology*, 7(2), 18-30
10. Meera N., Sood a. K., Chandrabhas N., and Ramakrishna J., “Raman study of lead borate glasses,” *J. Non. Cryst. Solids*, (1990). Vol. 126, pp. 224–230
11. M.F. Faznny, M.K. Halimah, C. Eevon, A.A. Latif, F.D. Muhammad, A.S. Asyikin, S.N. Nazrin, I. Zaitizila, Comprehensive study on the nonlinear optical properties of lanthanum nanoparticles and lanthanum oxide doped zinc borotellurite glasses, *Optics & Laser Technology*, Volume 127, 2020, 106161
12. Manara, Grandjean A., and Neuville D. R., “Structure of borosilicate glasses and melts: A revision of the Yun, Bray and Dell model,” *J. Non. Cryst. Solids*, (2009). Vol. 355, pp. 2528–2531
13. Khattak D. and Salim M. A., “X-ray photoelectron spectroscopic studies of zinc – tellurite glasses,” *Opt. Mater* (2002). Vol. 123, pp. 47–55
14. Y.S. Rammah, Ö.F. Özpolat, B. Alım, E. Şakar, R. El-Mallawany, F.I. El-Agawany, Assessment of gamma-ray attenuation features for La³⁺ co-doped zinc borotellurite glasses, *Radiation Physics and Chemistry*, Volume 176, 2020, 109069
15. V. Thomas, R.G.S. Sofin, M. Allen, H. Thomas, P.R. Biju, G. Jose, N.V. Unnikrishnan, Optical analysis of samarium doped sodium bismuth silicate glass, *Spectrochimica Acta Part A: Molecular and Biomolecular Spectroscopy*, Volume 171, 2017, Pages 144-148
16. José A. Jiménez, Sergiy Lysenko, Huimin Liu, Mariana Sendova, Luminescence of trivalent samarium ions in silver and tin co-doped aluminophosphate glass, *Optical Materials*, Volume 33, Issue 8, 2011, Pages 1215-1220

17. F. Ahmadi, R. Hussin, S.K. Ghoshal, Judd-Ofelt intensity parameters of samarium-doped magnesium zinc sulfophosphate glass, *Journal of Non-Crystalline Solids*, Volume 448, 2016, Pages 43-51
18. N.N. Yusof, S.K. Ghoshal, S.A. Jupri, M.N. Azlan, Synergistic effects of Nd³⁺ and Ag nanoparticles doping on spectroscopic attributes of phosphate glass, *Optical Materials*, Volume 110, 2020
19. Hidehiro Kamiya, Kuniaki Gotoh, Manabu Shimada, Tetsuo Uchikoshi, Yoshio Otani, Masayoshi Fuji, Shuji Matsusaka, Tatsushi Matsuyama, Junichi Tatami, Ko Higashitani, Kazue Kurihara, Naoyuki Ishida, Michitaka Suzuki, Hiroya Abe, Yasufumi Otsubo, Minoru Miyahara, CHAPTER 3 - CHARACTERISTICS AND BEHAVIOR OF NANOPARTICLES AND ITS DISPERSION SYSTEMS, Editor(s): Masuo Hosokawa, Kiyoshi Nogi, Mario Naito, Toyokazu Yokoyama, *Nanoparticle Technology Handbook*, Elsevier, 2008, Pages 113-176
20. Greenwood G. W., "The growth of dispersed precipitates in solutions," *Acta Metallurgica* (1956). Vol 4, pp. 56-70
21. Toy R., Hayden E., Shoup C., "The effect of particle size density and shape on margination of nanoparticles in microcirculation," *Nanotechnology*. (2011). Vol 22, pp. 43-54
22. Nanda K., Kundu R.S., Sharma S., Mohan D., "Study of vibrational spectroscopy, linear and non-linear optical properties of Sm³⁺ ions doped BaO-ZnO-B₂O₃ glasses." *Solid State Sciences*, (2015). Vol. 45, pp. 15-22
23. Y. Azlina, M.N. Azlan, M.K. Halimah, S.A. Umar, R. El-Mallawany, G. Najmi, Optical performance of neodymium nanoparticles doped tellurite glasses, *Physica B: Condensed Matter*, Volume 577, 2020, 411784
24. Hagar Elkholy, Hosam Othman, Ibrahim Hager, Medhat Ibrahim, Dominique de Ligny, Thermal and optical properties of binary magnesium tellurite glasses and their link to the glass structure, *Journal of Alloys and Compounds*, Volume 823, 2020, 153781
25. S.H. Elazoumi, H.A.A. Sidek, Y.S. Rammah, R. El-Mallawany, M.K. Halimah, K.A. Matori, M.H.M. Zaid, Effect of PbO on optical properties of tellurite glass, *Results in Physics*, Volume 8, 2018, Pages 16-25,
26. C. Devaraja, G.V. Jagadeesha Gowda, B. Eraiah, Optical Properties of Bismuth Tellurite Glasses Doped with Holmium Oxide, *Ceramics International*, 2020
27. M.N. Azlan, M.K. Halimah, A.B. Suriani, Y. Azlina, S.A. Umar, R. El-Mallawany, Upconversion properties of erbium nanoparticles doped tellurite glasses for high efficient laser glass, *Optics Communications*, Volume 448, 2019, Pages 82-88
28. M.N. Azlan, M.K. Halimah, A.B. Suriani, Y. Azlina, R. El-Mallawany, Electronic polarizability and third-order nonlinearity of Nd³⁺ doped borotellurite glass for potential optical fiber, *Materials Chemistry and Physics*, Volume 236, 2019, 121812
29. M.S.A. Mohd Saidi, S.K. Ghoshal, K. Hamzah, R. Arifin, M.F. Omar, M.K. Roslan, E.S. Sazali, Visible light emission from Dy³⁺ doped tellurite glass: Role of silver and

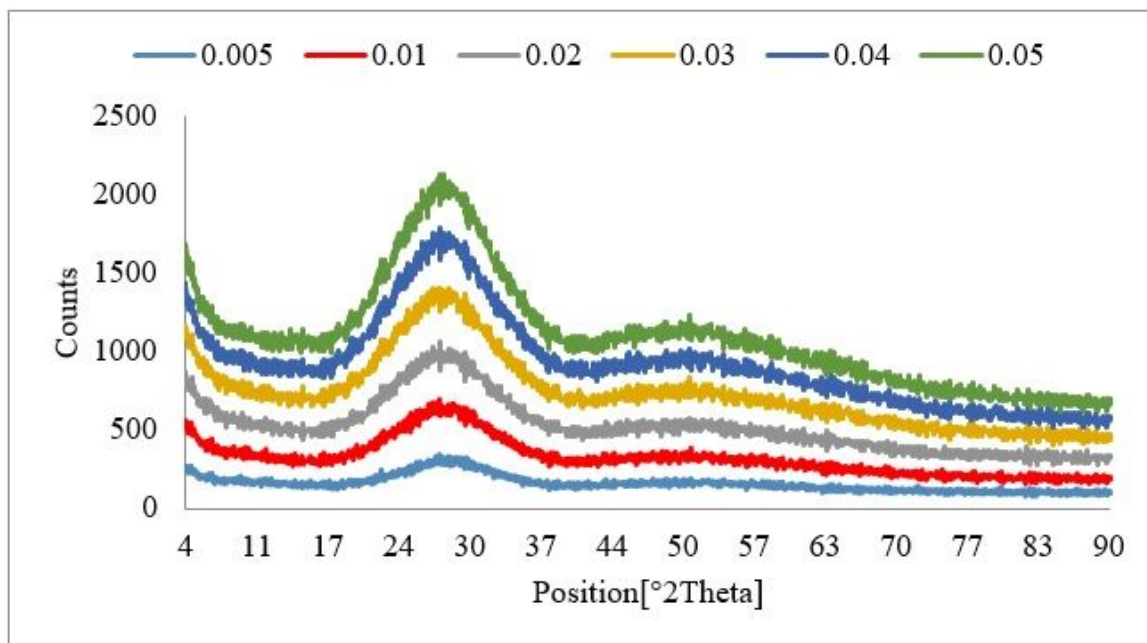
titanium nanoparticles co-embedding, *Journal of Non-Crystalline Solids*, Volume 502, 2018, Pages 198-209

30. Eevon, C., Halimah, M.K., Azlan, M.N., El-Mallawany, R., & Hii, S.L. (2019). Optical and thermal properties of TeO₂–B₂O₃–Gd₂O₃ glass systems, *Materials Science-Poland*, 37(4), 517-525
31. Ahlawat N., Sanghi S., Agarwal A. and Rani S “Effect of Li₂O on structure and optical properties of lithium bismosilicate glasses.” *Journal of Alloys and Compounds*. (2009). Vol. 480, pp. 516-520
32. Abdel-Baki M and El-Diasty F. “Optical Properties of Oxide Glasses containing Transition Metals.” *Current Opinion in Solid State and Materials Science*. (2006). Vol. 34, pp. 217-229
33. Gupta P., Ramrakhiani M., “Influence of the particle size on the optical properties of CdSe nanoparticles,” *The Open Nanoscience Journal*. (2009). Vol 3, pp. 15-19
34. Kassab R.P., Camilo M. E., Amâncio C. T., Da Silva D. M., and Martinelli J. R. “Effects of gold nanoparticles in the green and red emissions of TeO₂–PbO–GeO₂ glasses doped with Er³⁺–Yb³⁺,” *Opt. Mater.* (2011). Vol. 33, pp. 1948–1951
35. Qi Y., Zhou Y., Wu L., Yang F., Peng S., Zheng S., and Yin D., “Silver nanoparticles enhanced 1.53 μm band fluorescence of Er³⁺ / Yb³⁺ codoped tellurite glasses,” *Journal of Luminescence*. (2014). Vol. 153, pp. 401–407
36. Dimitrov V., Komatsu T., “Electronic polarizability, optical basicity and non-linear optical properties of oxide glasses”. *Journal of Non-crystalline Solids*. (1999). Vol. 249, pp. 169-179
37. M.K. Halimah, M.F. Faznny, M.N. Azlan, H.A.A. Sidek, Optical basicity and electronic polarizability of zinc borotellurite glass doped La³⁺ ions, *Results in Physics*, Volume 7, 2017, Pages 581-589,
38. H.H. Smaili, H. Algarni, Shoroog Alraddadi, Y.S. Rammah, Tanin Nutaro, M.S. Al-Buriah, Mechanical, optical, and beta/gamma shielding properties of alkali tellurite glasses: Role of ZnO, *Ceramics International*, Volume 46, Issue 18, Part A, 2020, Pages 28594-28602
39. Imed Boukhris, Imen Kebaili, M.I. Sayyed, A. Askin, Y.S. Rammah, Linear, nonlinear optical and photon attenuation properties of La³⁺ doped tellurite glasses, *Optical Materials*, Volume 108, 2020, 110196

Figures



a



b

Figure 1

a XRD spectra for ZBTsm-MPs glass series. b XRD spectra for ZBTsm-NPs glass series

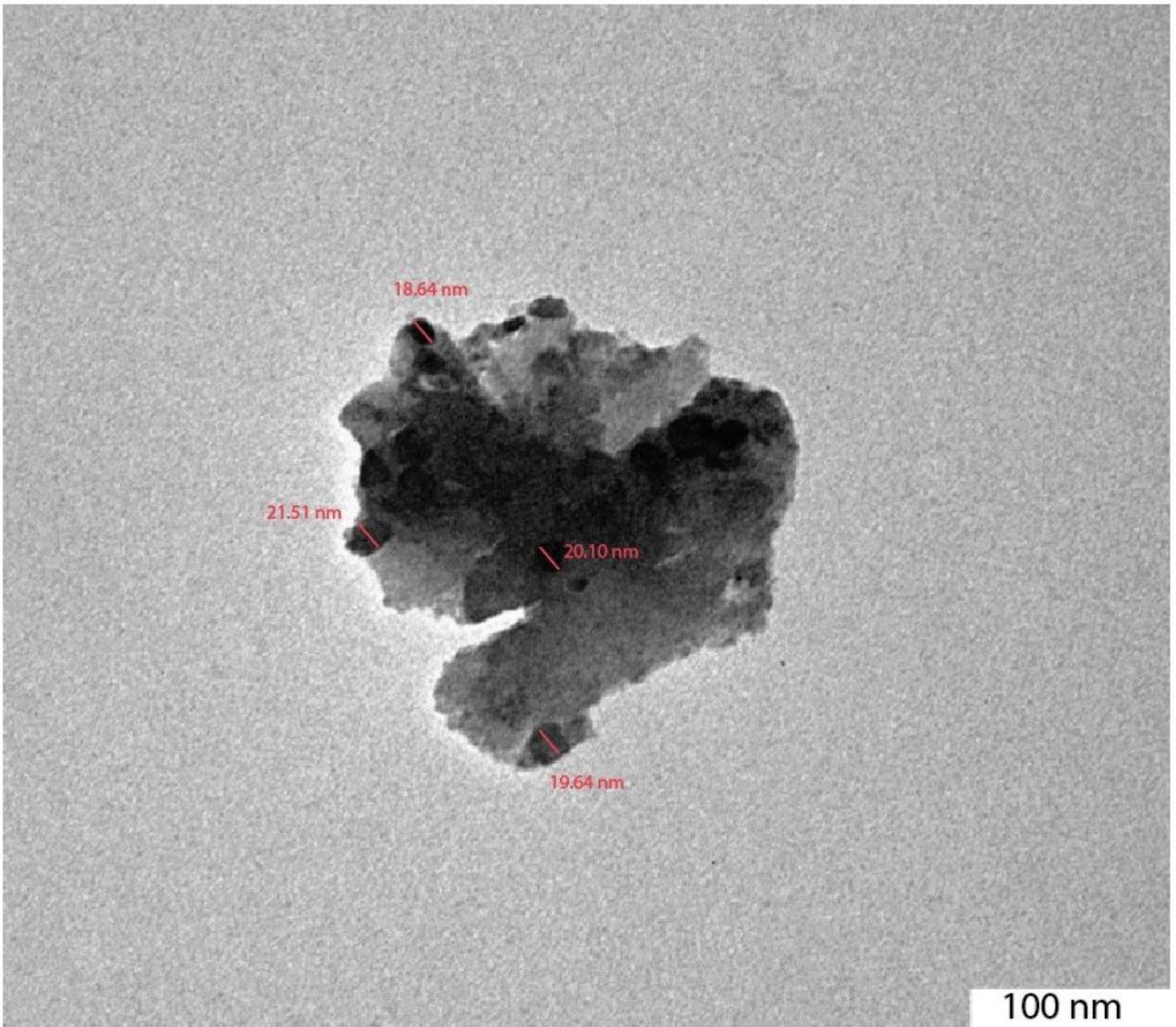


Figure 2

TEM micrograph image for ZBTsm-NPs glass series

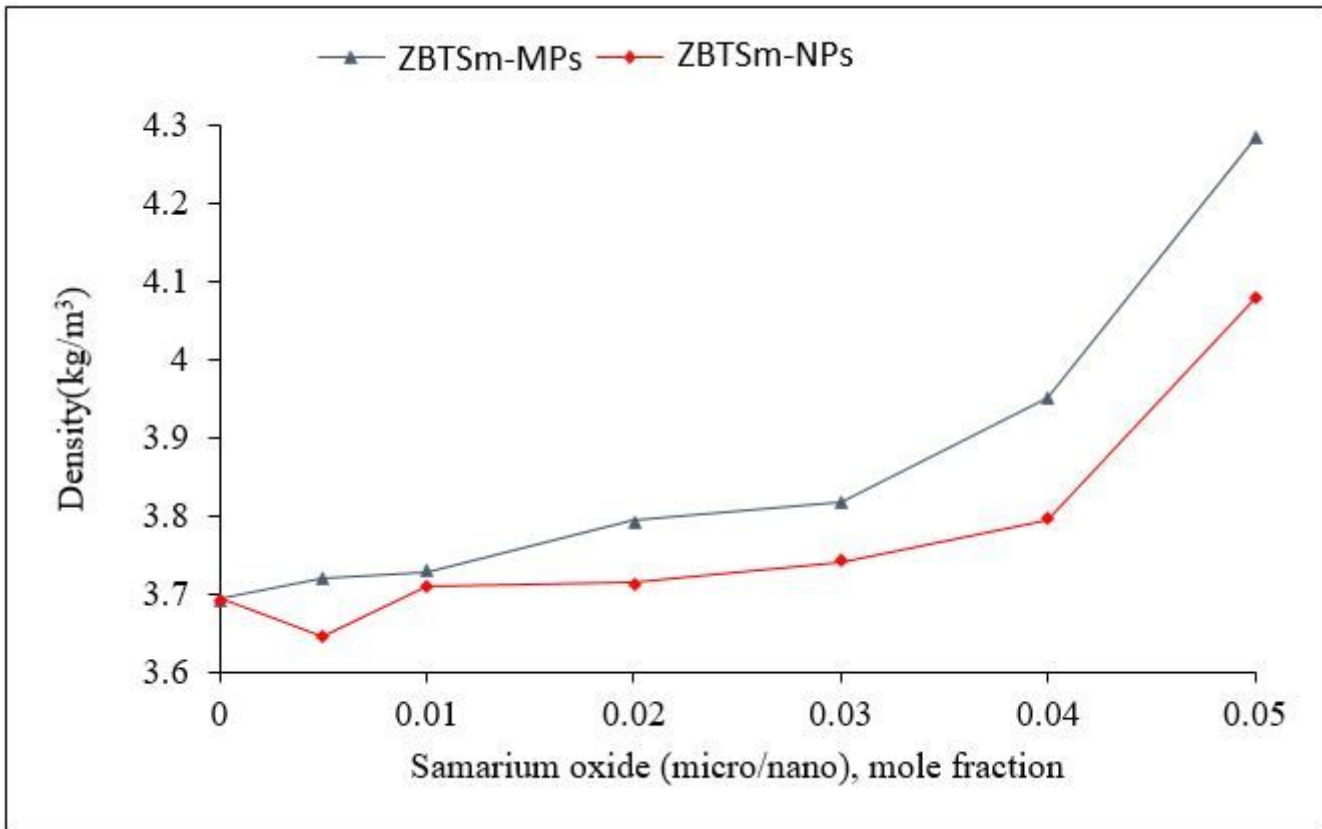


Figure 3

Density for ZBTSm-MPs and ZBTSm-NPs glass series

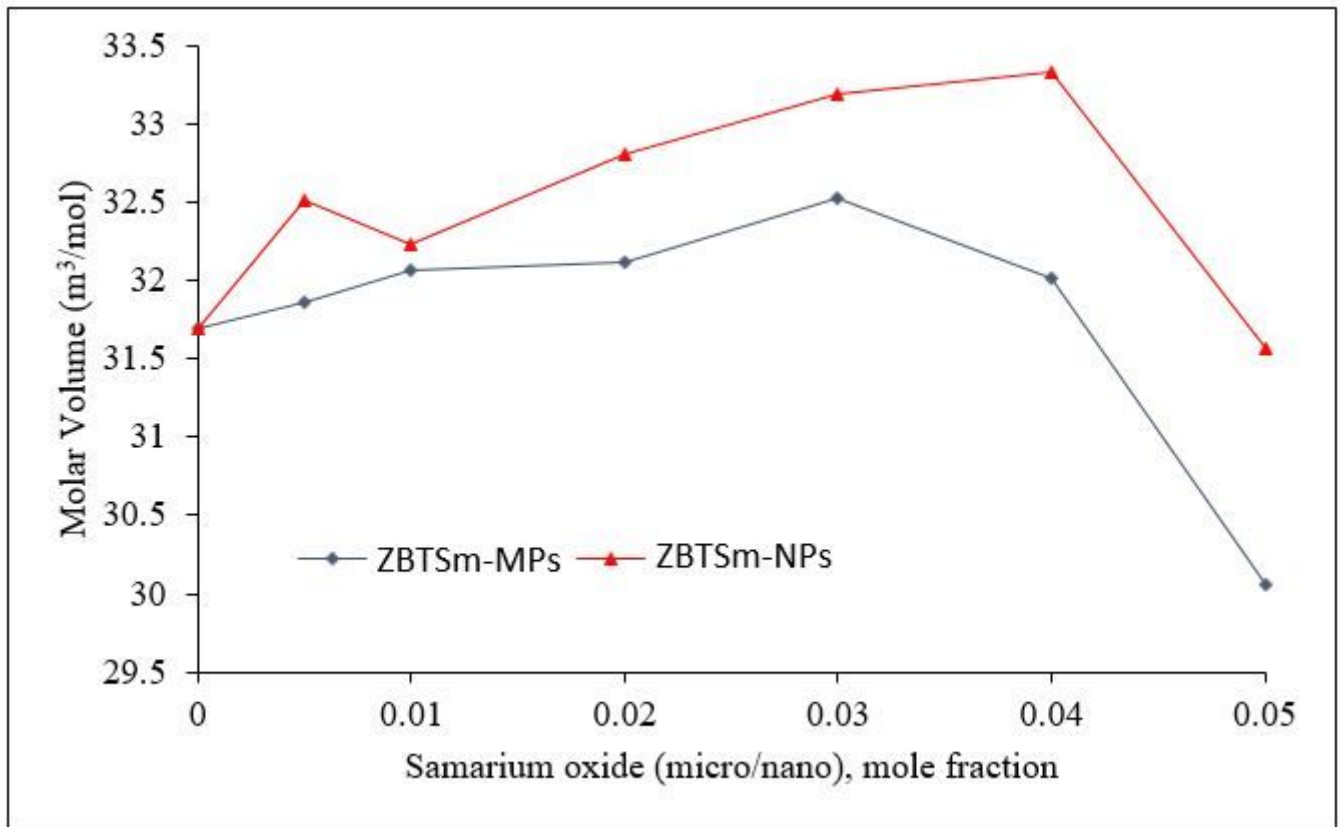


Figure 4

Molar volume for ZBTsm-MPs and ZBTsm-NPs glass series

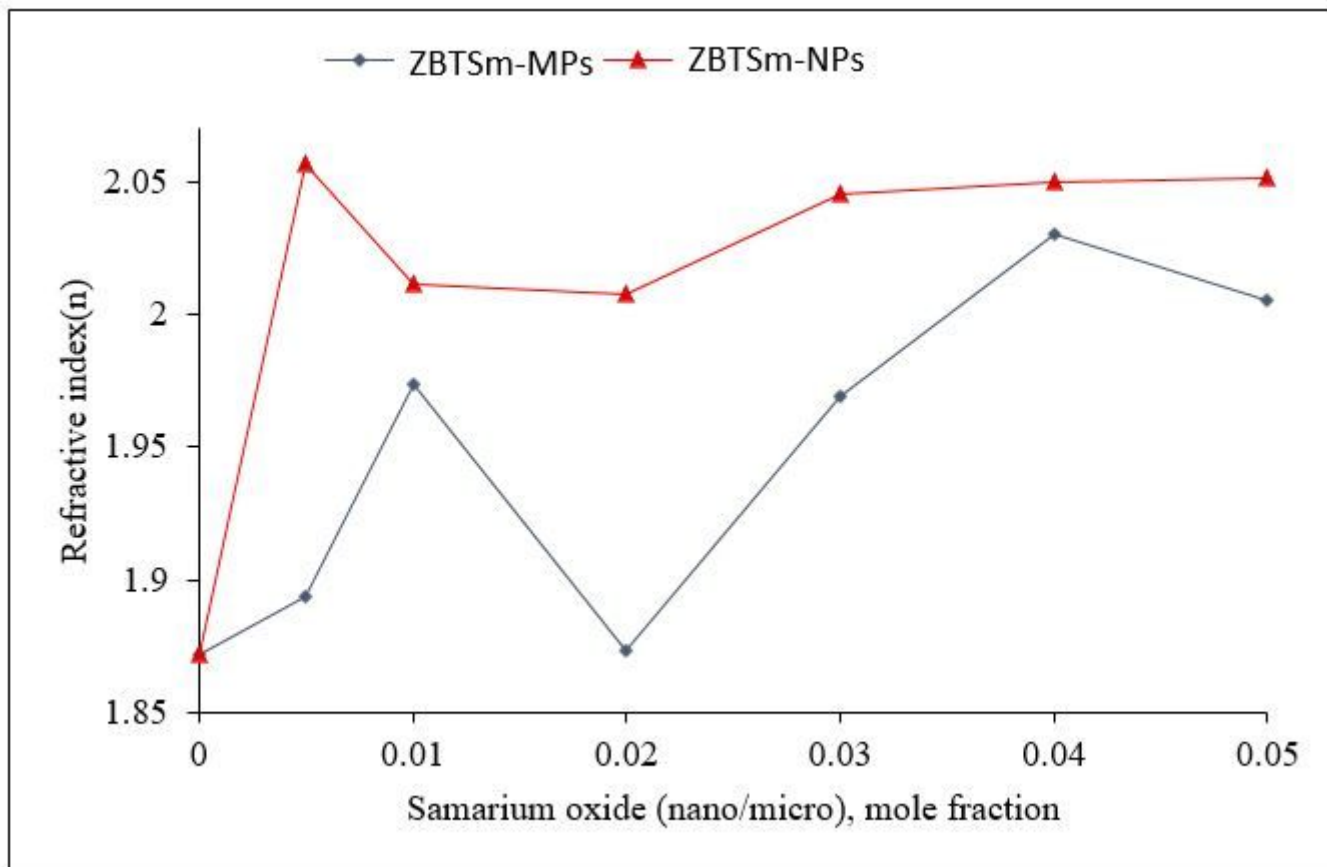


Figure 5

Refractive index for ZBTSm-MPs and ZBTSm-NPs glass series

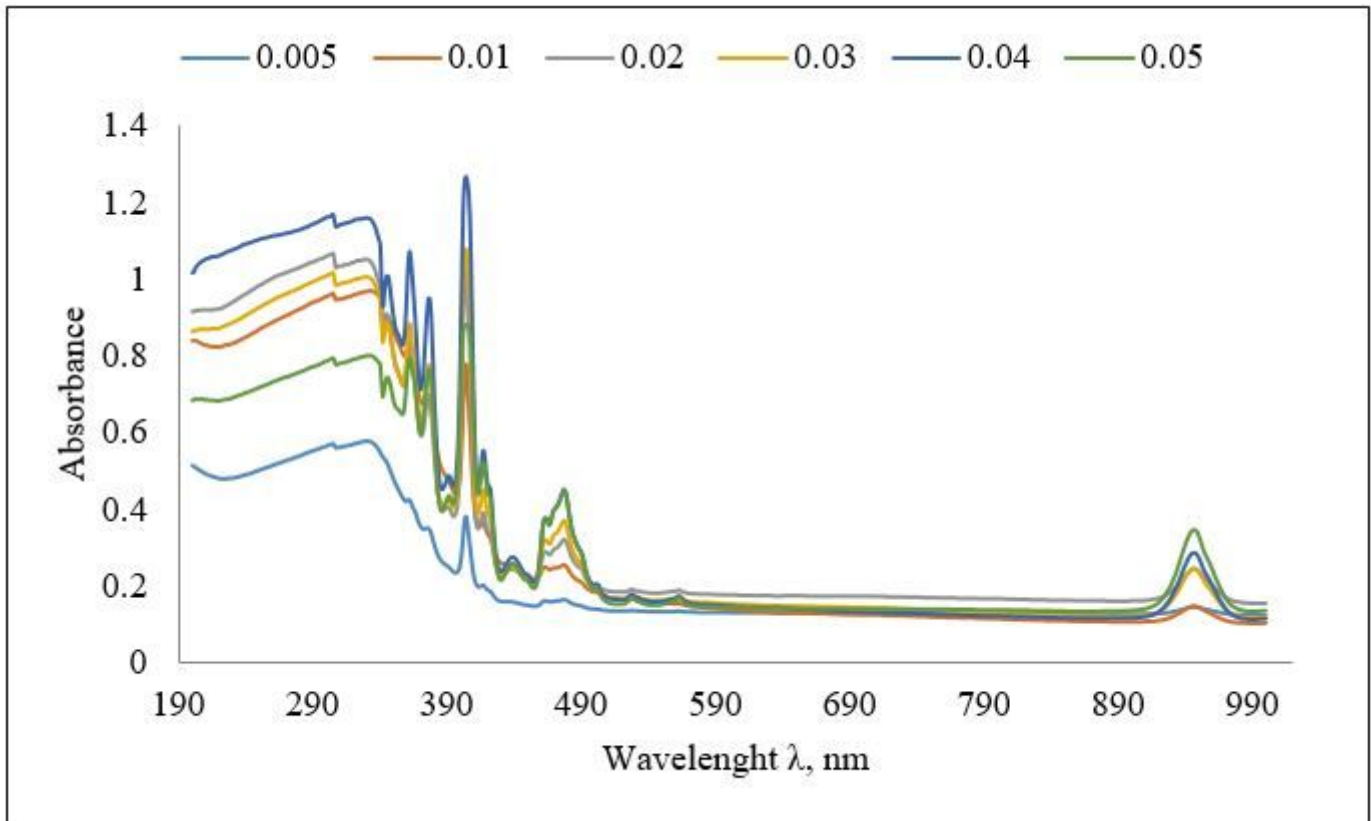


Figure 6

Optical absorption for ZBTsm-MPs glass series

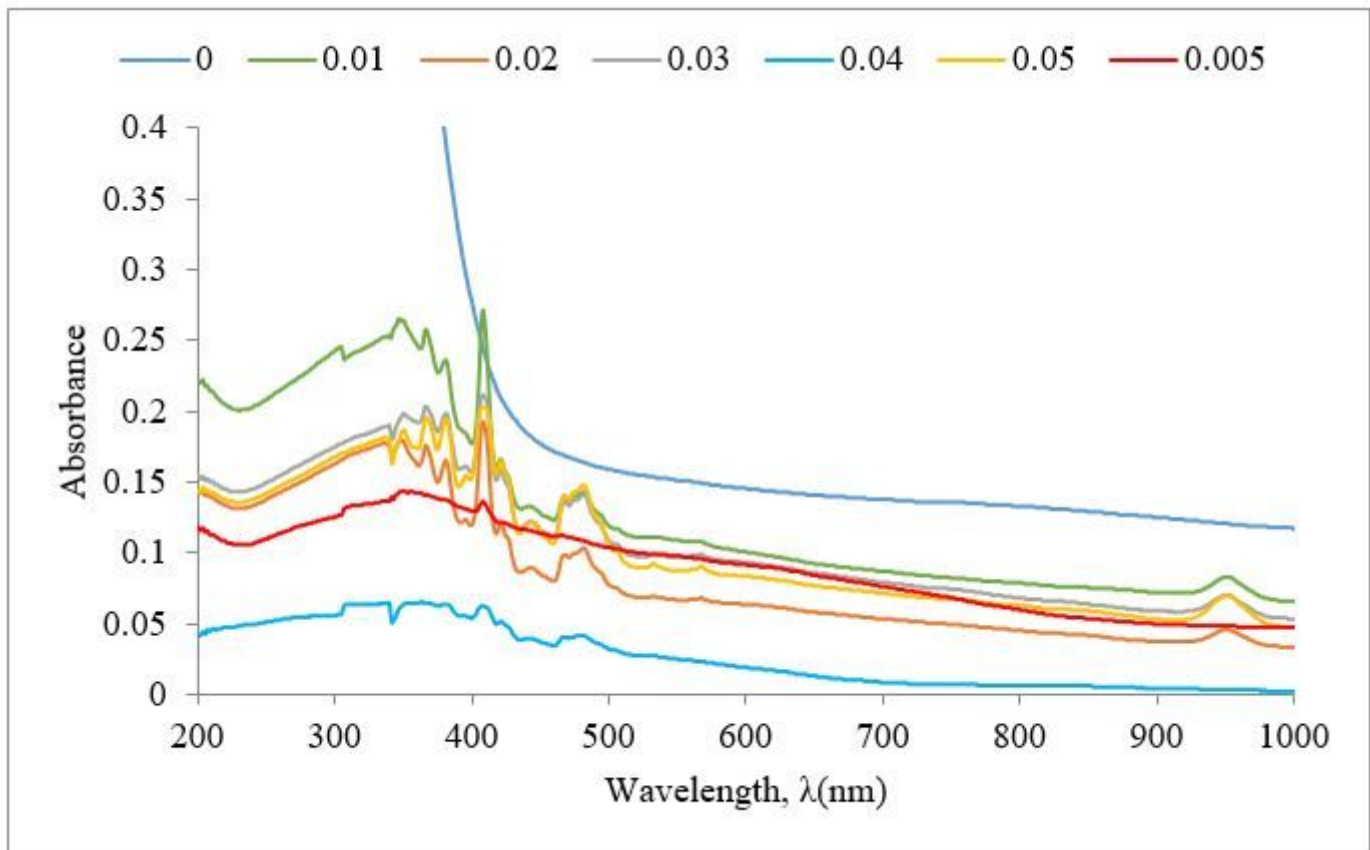


Figure 7

Optical absorption for ZBTsm-NPs glass series

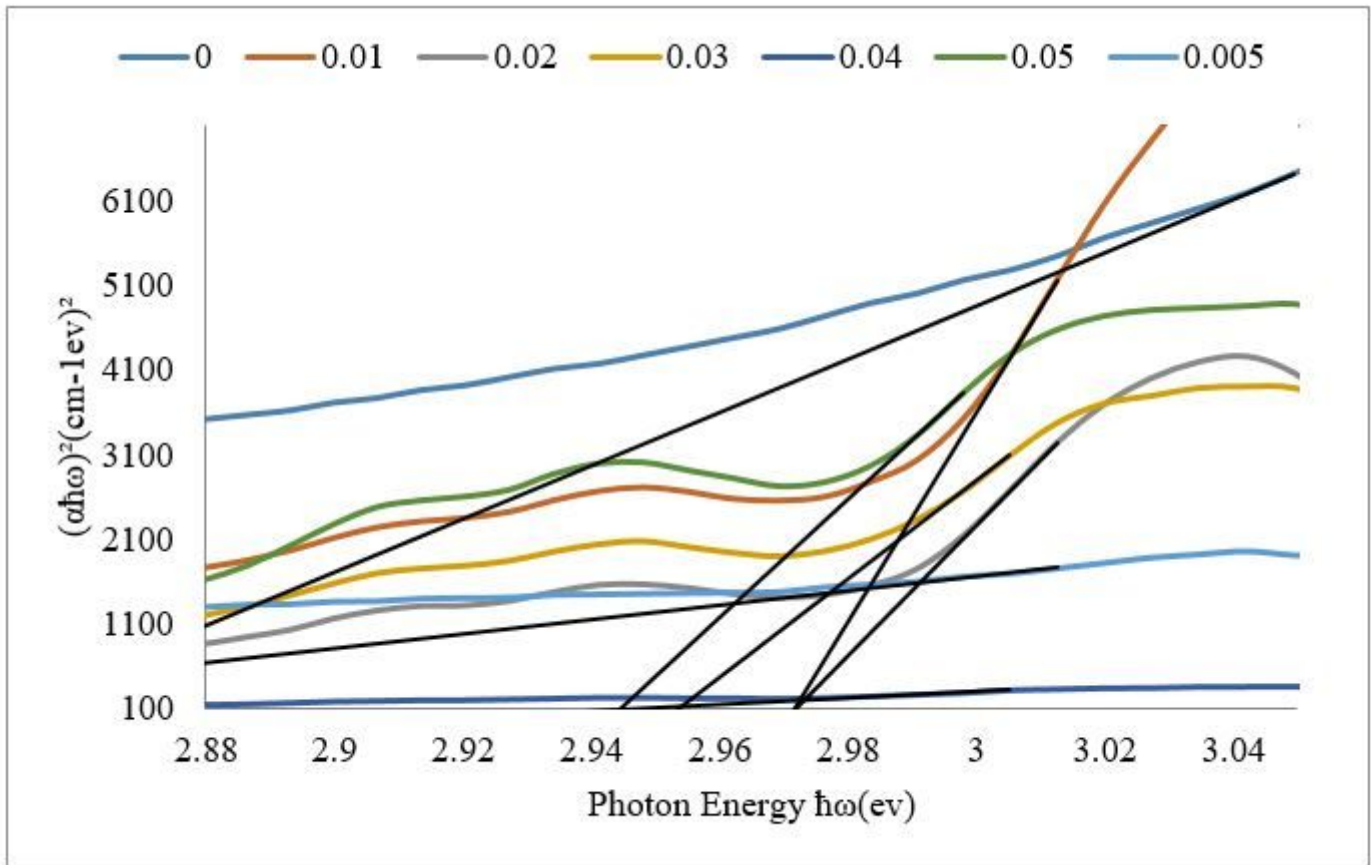


Figure 8

Plot of $(\alpha\hbar\omega)^2$ against photon energy $\hbar\omega$ of ZBTsm-MPs for direct band gap measurement

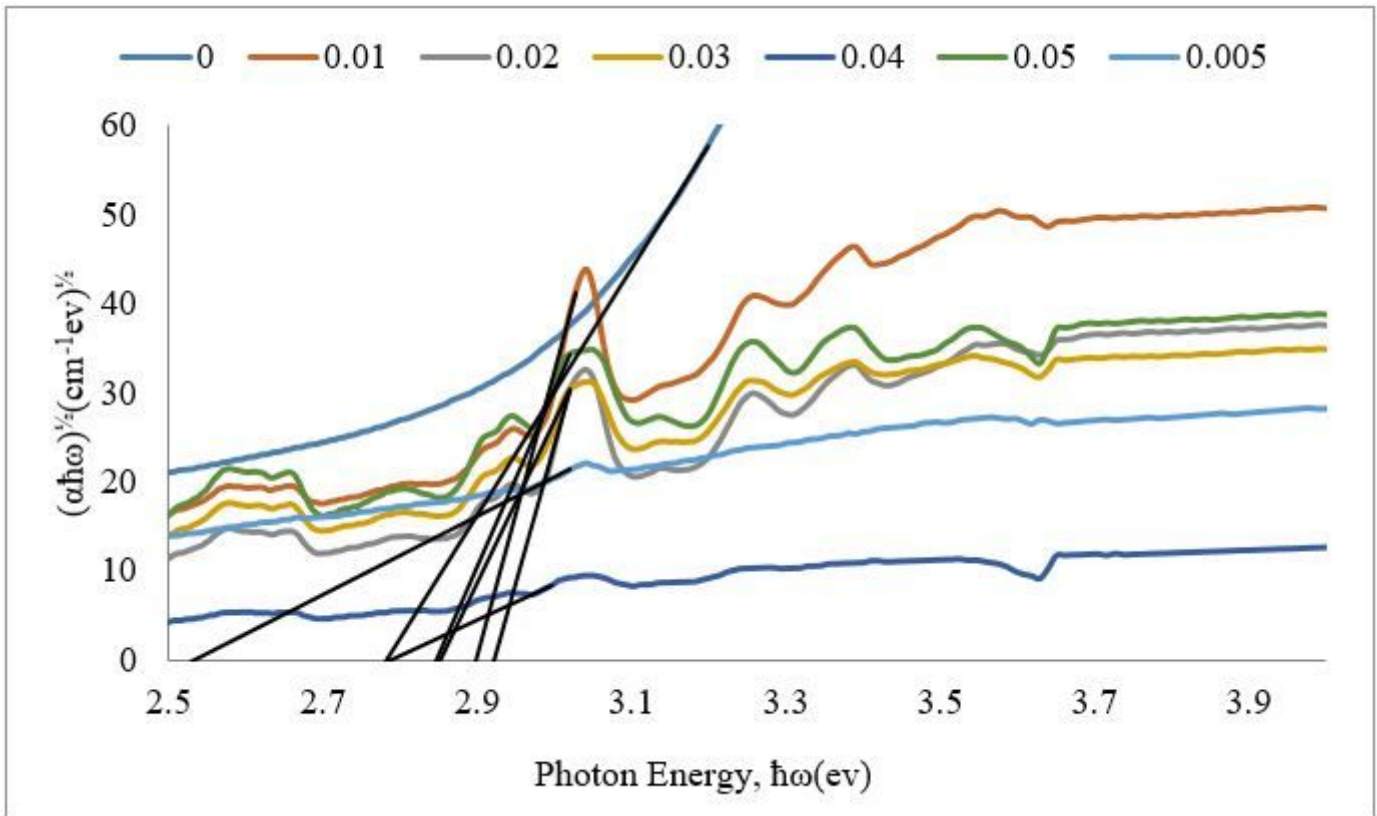


Figure 9

Plot of $(\alpha\hbar\omega)^{1/2}$ against photon energy $\hbar\omega$ of ZBTSm-MPs for indirect band gap measurement

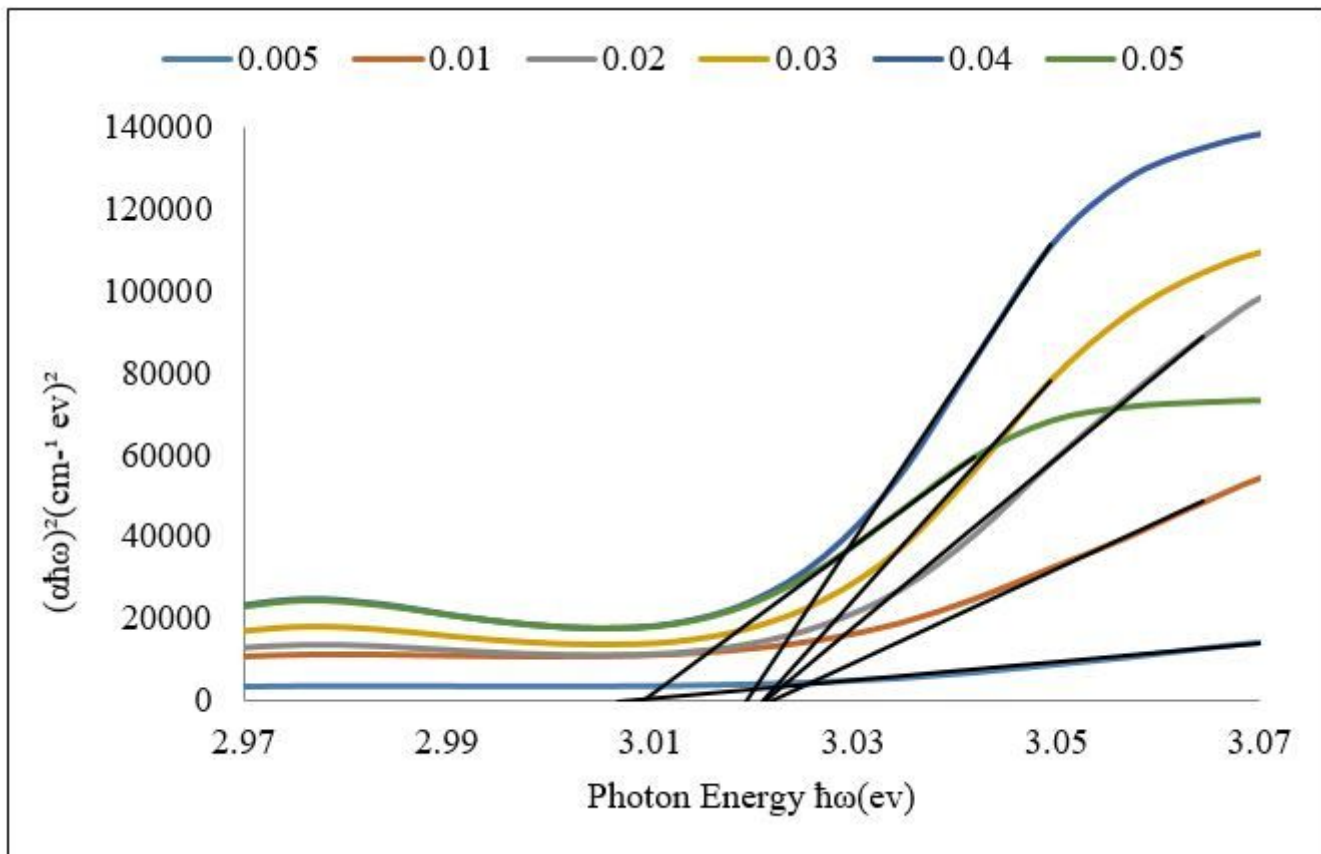


Figure 10

Plot of $(\alpha\hbar\omega)^2$ against photon energy $\hbar\omega$ of ZBTsm-NPs for direct band gap measurement

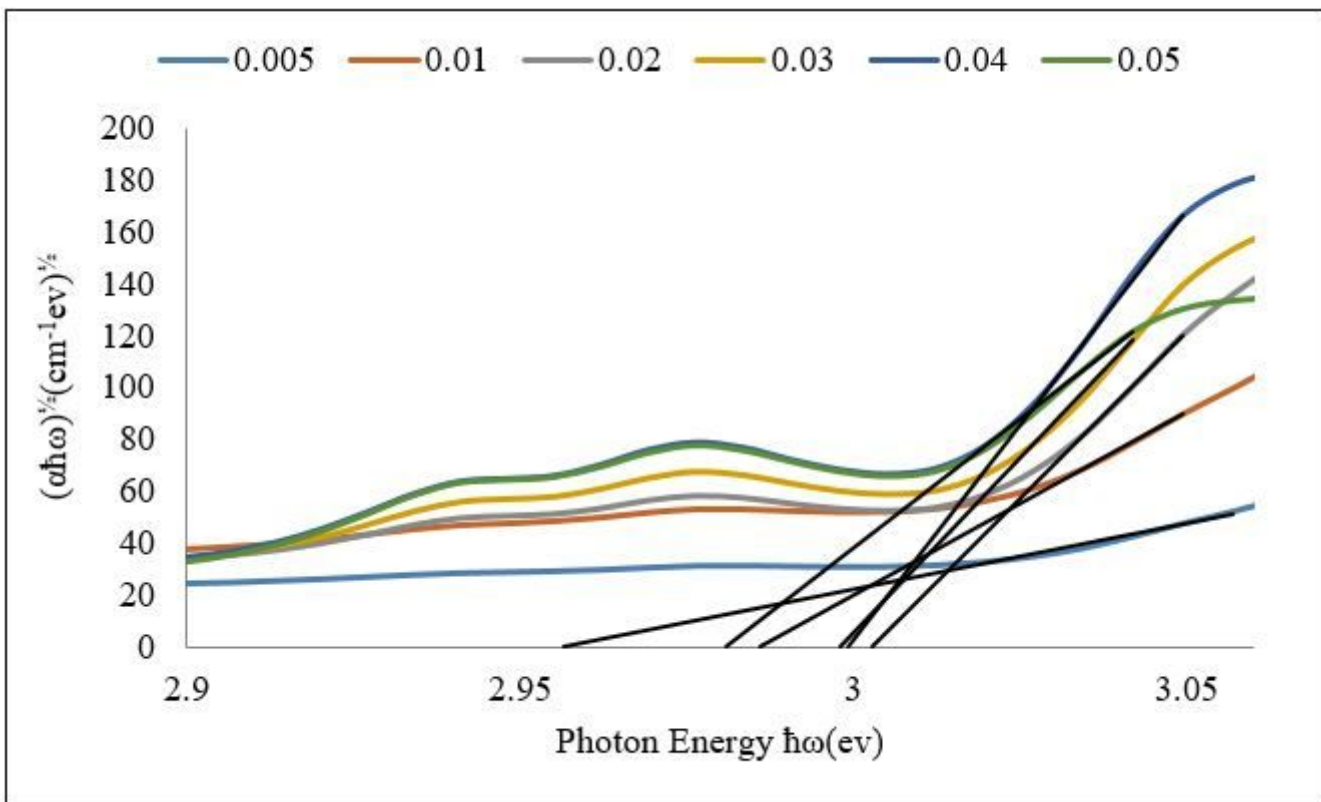


Figure 11

Plot of $(\alpha\hbar\omega)^{1/2}$ against photon energy $\hbar\omega$ of ZBTSm-NPs for indirect band gap measurement

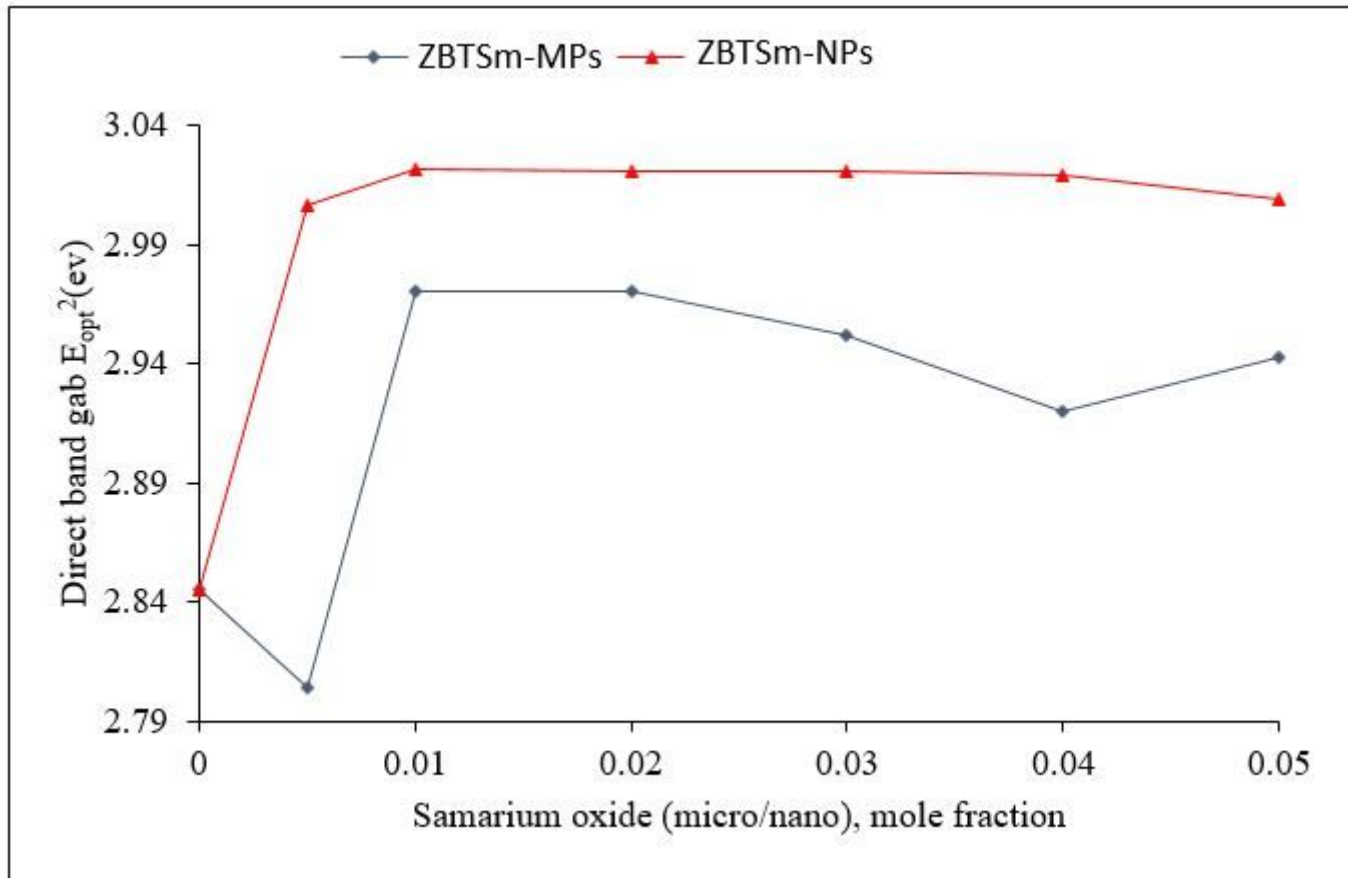


Figure 12

Direct optical band gap for ZBTSm-MPs and ZBTSm-NPs glass series

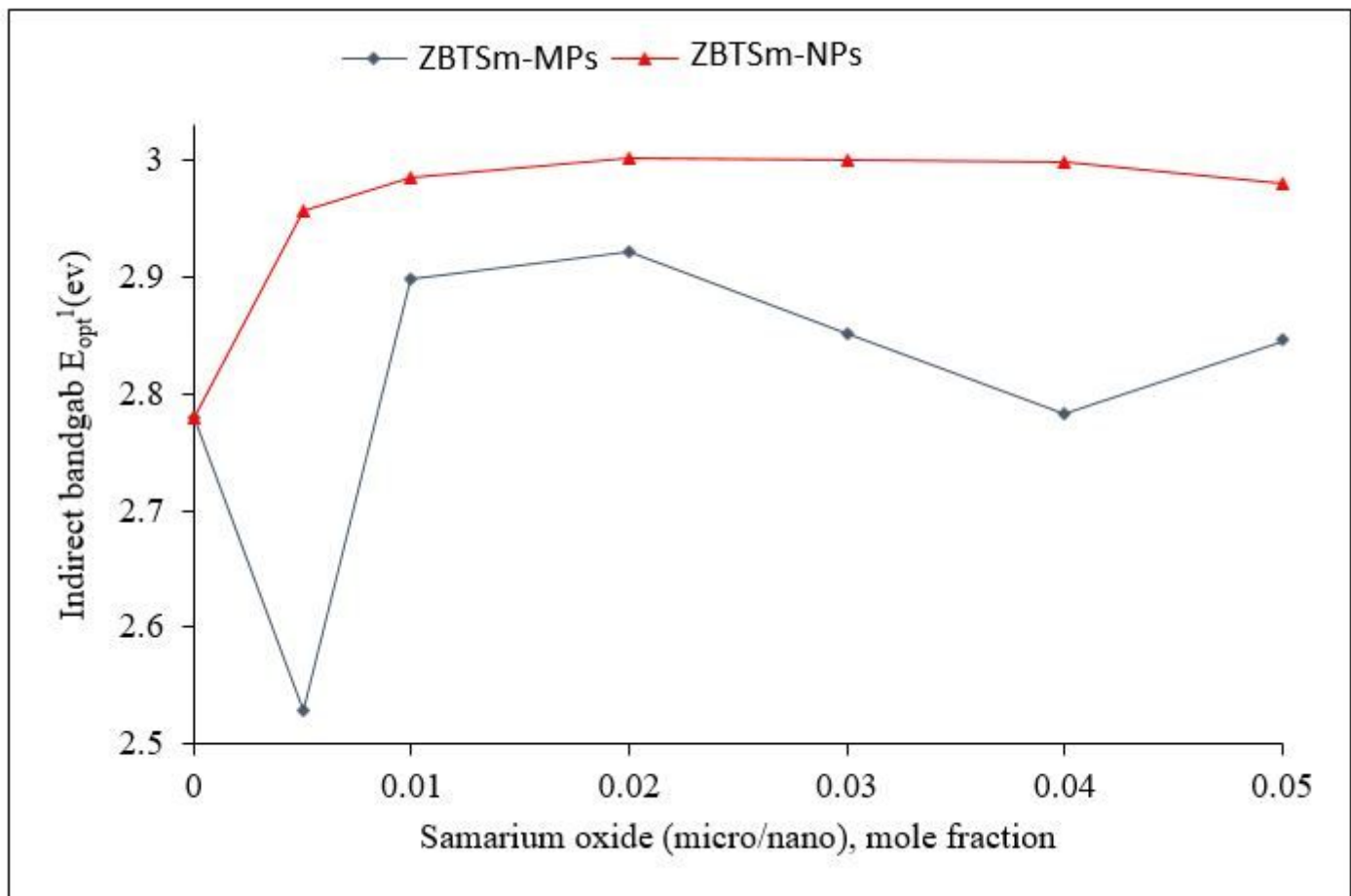


Figure 13

Indirect optical band gap for ZBTsm-MPs and ZBTsm-NPs glass series

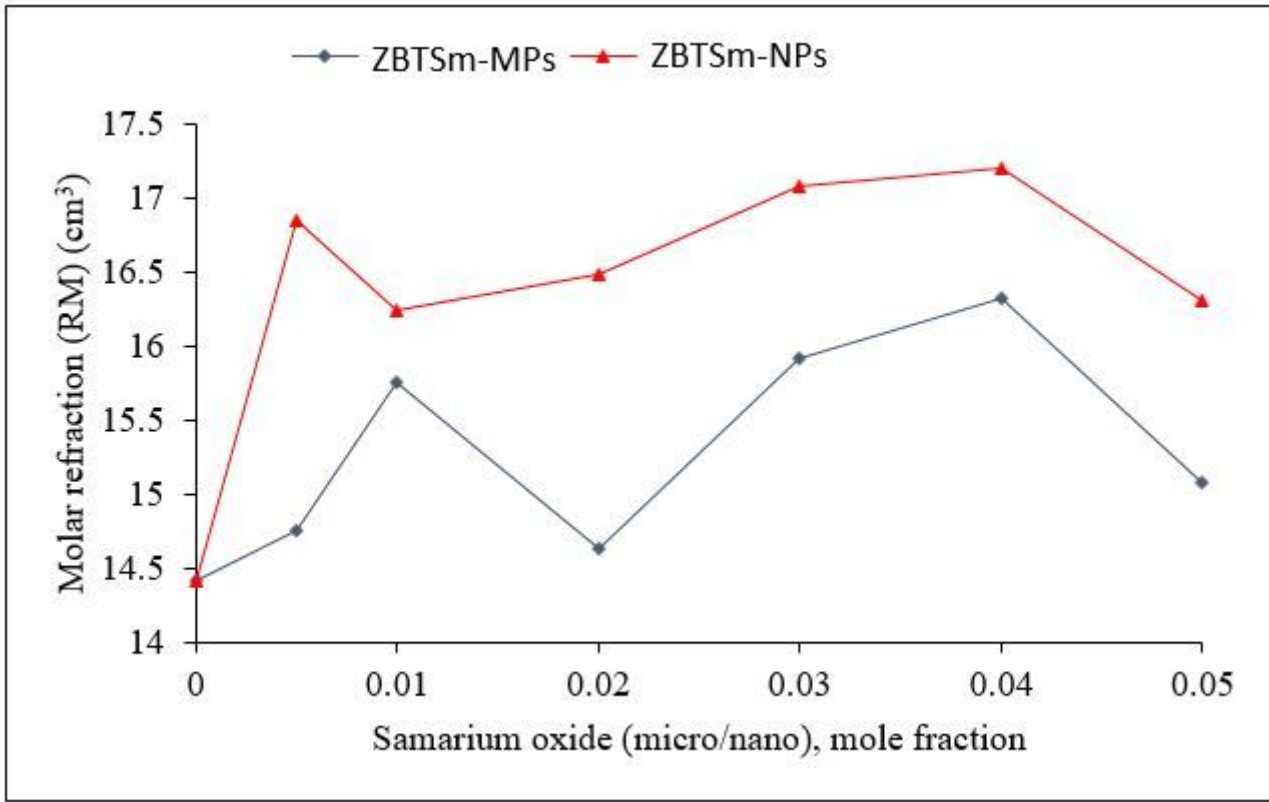


Figure 14

Molar refraction for ZBTsm-MPs and ZBTsm-NPs glass series

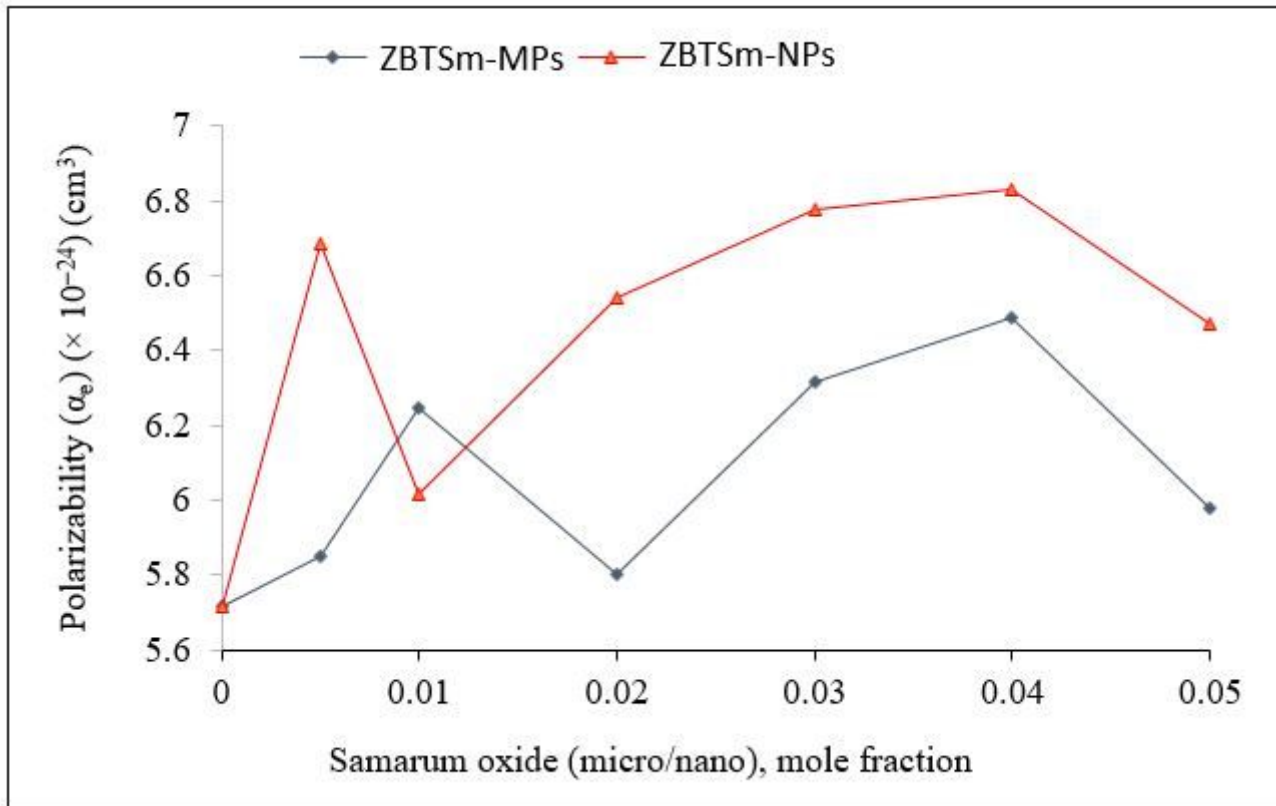


Figure 15

Polarizability for ZBTSm-MPs and ZBTSm-NPs glass series